Biomechanical Behaviour of Bone-Implant Interface: A Review

Xing Gao, Manon Fraulob, Guillaume Haïat

Biomechanical Behaviours of the Bone-Implant Interface: A Review

Xing Gao[1, 2], Manon Fraulob[1] and Guillaume Haïat[1, *]

[1] CNRS, Laboratoire Modélisation et Simulation Multi Echelle, UMR CNRS 8208, 61 avenue du Général de Gaulle, 94010 Créteil cedex, France

[2] Research Centre for Medical Robotics and Minimally Invasive Surgical Devices, Shenzhen Institutes of Advanced Technology, Chinese Academy of Sciences, Shenzhen 518055, China

Corresponding author: Guillaume Haïat (guillaume.haiat@univ-paris-est.fr)

Abstract

In recent decades, cementless implants have been widely used in clinical practice to replace missing organs, to replace damaged or missing bone tissue or to restore joint functionality. However, there remain risks of failure which may have dramatic consequences. The implant success depends on the implant stability that is determined by the biomechanical properties of the bone-implant interface (BII). The aim of this review article is to provide more insight on the current state of the art concerning the evolution of the biomechanical properties of the BII as a function of the implant environment.

The main characteristics of BII and the determinants of the implant stability are first introduced. Then, the different mechanical methods that have been employed to derive the macroscopic properties of the BII will be described. The experimental multimodality approaches used to determine the microscopic biomechanical properties of periprosthetic newly formed bone tissue are also reviewed. Eventually, the influence of the implant properties, both in terms of surface properties and of biomaterials are investigated. A better understanding of the phenomena occurring at the BII will lead i) to medical devices helping the surgeon measuring the implant stability and ii) to improve the quality of implants.

Key words: Biomechanical behaviour, bone-implant interface, mechanical measurement, stability, cementless

1. Introduction

Population ageing and the occurrence of road traffic, sports and work accidents are the main reasons explaining the increasing interest of the research community in studying the osteoarticular system. Implanting biomaterials within bone tissue to restore the functionality of the treated organ has become a common technique in orthopaedic and dental surgery [1]. Implants and articular prostheses have led to important progress in the repair of joint degeneration (hip, knee…) and in maxillofacial surgery (to restore missing teeth or support craniofacial reconstructions). Modern orthopaedic and dental implant treatments aim at a rapid strong and long-lasting attachment between implant and bone tissue.

Despite their routine clinical use, implant failures still occur and remain difficult to anticipate as the reasons for implant losses remain unclear. The surgical success of implant surgeries depends on the evolution of the biomechanical properties of the bone-implant interface (BII), which remains difficult to determine *in vivo*. Predicting implant failure is difficult because bone is a complex multi-scale medium evolving as a function of time through remodelling phenomena. Moreover, the presence of an interface complicates the situation. Another difficulty arises from the fact that the implant success depends on multifactorial aspects related to the patients (e.g.: behaviour, bone quality…), to the surgeons (e.g. aseptic conditions during surgery, surgical and loading protocol…) and to the implant manufacturers (e.g. implant surface, biomaterial, implant geometry…).

Bone is a strong and lightweight composite multi-scale anisotropic material which presents a hierarchy of microstructures [2]. At the scale of several hundred nanometres, mineralised bone is composed of elementary components such as hydroxyapatite, cylindrically shaped collagen molecules and water. At the scale of 1–10 µm, bone is constituted by the ultrastructure, composed of collagen fibres and extrafibrillar spaces. At the scale of several hundred micrometres to several millimetres, the microstructure depends on the type of bone.

Besides its multi-scale nature, bone can adapt its structure through remodelling phenomena [3], which induces changes of its structure and mechanical properties to accommodate itself for presence of the implant. A better understanding of the biomechanical properties of newly formed bone around the implant interface may lead to more accurate prediction of the surgical outcome of implant integration [4], preventing additional painful and expensive surgical interventions.

Implant retention is determined by interfacial phenomena such as friction or mechanical interlocking. Surface roughness influences its mechanical stability [5]. Rough surface structures may stimulate the repair of bone tissue [6] and may also introduce mechanically based effects in bone, such as interlocking due to bone growth into the surface [7].

Despite the aforementioned difficulties, the industrial design of implants has often been driven by an aggressive "copycat" marketing approach rather than by fundamental advances in biomechanics [8]. Clinicians have often used implants in new applications before research has been carried out from a basic science viewpoint. Empirical approaches are limited to understand the interaction of the mechanisms determining osseointegration phenomena.

To date, cemented and cementless implants are the two main types of implants used in orthopedic surgery, while to the best of our knowledge, bone cement is not used for the anchorage of oral implants. Although bone cement, acting as a bonding medium, can provide initial fixation, cementless implants are now more and more often preferred due to risks of cemented implant failures related to an accumulation of micro-cracks in and around the cemented area [9]. Moreover, systemic risks such as cement implantation syndrome during and after cementation procedure have been noticed [10]. Consequently, this work focused only on cementless implants where bone tissue is in direct contact with the implant surface.

The aim of this review is to provide the state of the art on the evolution, the measurement and the dependence of the biomechanical properties of the BII, which is important because i) it is related to the implant primary and secondary stability and ii) the BII is suggested to be the weakest domain in bone-implant system where most failures occur [11].

In this review, we chose to focus on aspects related to biomechanics. Readers interested in biological or biochemical aspects are referred to other publications, such as for example [12-18]. An introduction on the description of the evolution of the biomechanical properties of the BII and on its relation with the implant stability will be given in section 2. Then, various methods used to assess the biomechanical properties of the BII at the macroscopic scale will be described, such as mechanical tests with tensile, shear, torque and friction tests. Then, different experimental techniques aiming at determining the microscopic biomechanical properties of newly formed bone tissue will be investigated. Eventually, the influence of the environment such as the type of biomaterial and the surface roughness on the biomechanical properties of the BII will be investigated.

2. Implant stability

The biomechanical properties of the BII are determinant for the implant stability. A good quality of bone healing leads to: i) direct contact between mineralised bone tissue and the implant and ii) an important proportion of the implant surface in intimate contact with bone tissue. The success of implant surgery is determined by the biomechanical quality of bone tissue located at a distance lower than around 100-200 µm from the implant surface [19, 20]. The quantity is also an important parameter for the surgical success, even if Bolind *et al.* [21] reported that the the bone-implant contact ratio (BIC) in successful oral implants varied between 60 and up to 99% with no evidence whatsoever that those implants with 99% BIC fared any better than those with 60%. The BIC ratio is correlated with the biomechanical properties of BII and it increases during bone healing [20, 22] as firstly described by Johansson and Albrektsson in 1987 [23].

Figure 1 describes schematically the evolution of the BII as a function of healing time, known as *osseointegration* phenomena that were first defined by Brånemark in 1976 [24]. Just after surgery (Fig. 1a), the implant surface is surrounded by blood (due to the reaming of the bone cavity), dead and living bone tissue. Bone debris may also be present around the implant

surface. During bone healing, which occurs several weeks / months after surgery, newly formed bone is produced to fill the gap between mature bone tissue and the implant surface (Fig. 1b). Several weeks or months after the implant surgery, newly formed bone tissue is replaced progressively by mature bone tissue around the implant surface, leading to the final BIC ratio as shown in Fig. 1c.

Histological analysis is the gold standard to determine the BIC but it cannot be used in clinical practice. Classical X-ray based techniques [25] and magnetic resonance imaging [26] cannot be used to assess the BIC because of metal artefacts related to the presence of titanium [25].

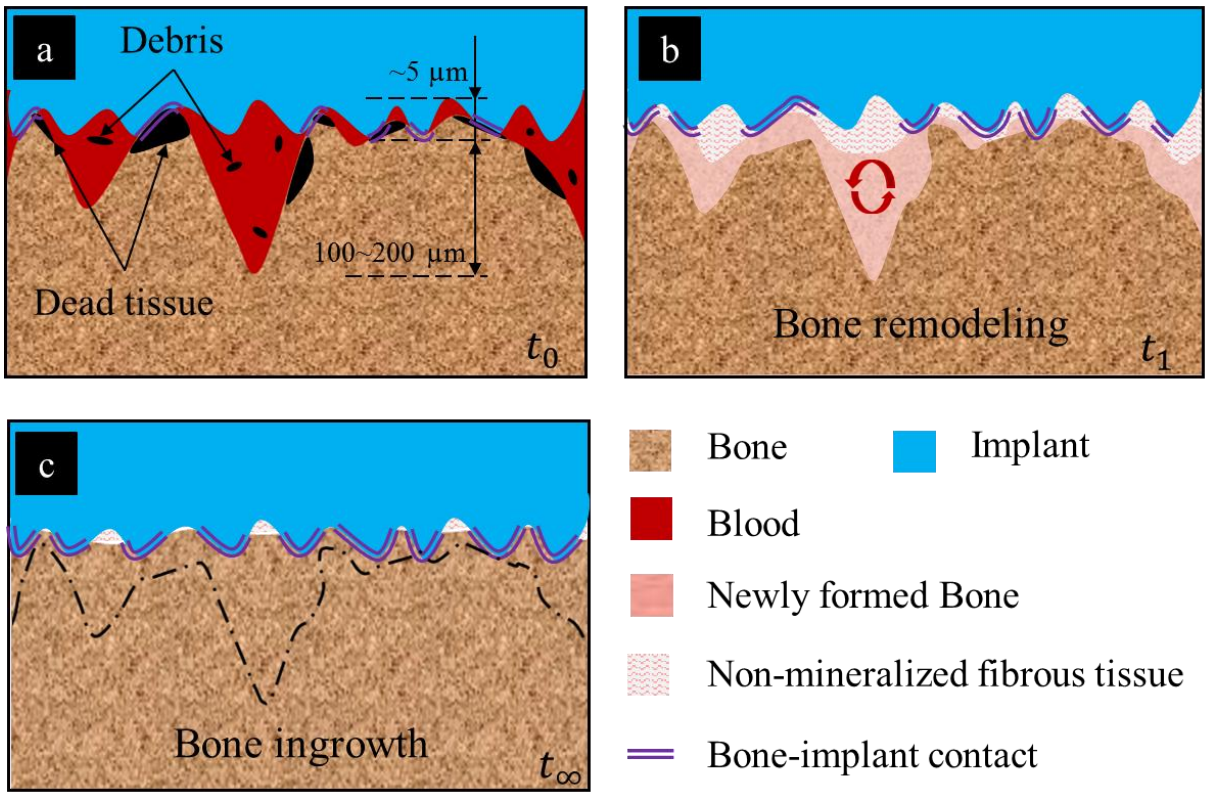

Figure 1: Schematic representation of bone-implant interface (a) immediately after surgery (time t_0), (b) during the bone remodelling period t_1(formation of newly formed bone) and (c) after completion of osseointegration t_∞.

2.1.Primary stability of cementless implant

Cementless implants can be either screwed home in bone tissue (which is the case for dental implants and some orthopedic implants), or inserted in bone tissue using the "press-fit" technique (for orthopedic implants), which consists in introducing the implant into a cavity (slightly smaller than the implant size) formed by drilling or cutting, thus leading to the implant primary stability through the pre-stressed state of bone tissue [27-29]. Frictional properties of the BII are then determinant to ensure a proper implant stability at early post-

operative stages (see subsection 3.2). Primary stability is defined as the stability of the implant just after the surgical insertion, before the healing period.

Friction phenomena between the implant surface and bone tissue are used to sustain shear load at the BII [30] (e.g. at the tibia [31], hip [32], femur [33], glenoid [34], etc.). Screwing may also be important to provide mechanical fixation (e.g. dental [19], spinal devices [35], intramedullary rods [36], etc.). Although surgery may damage bone tissue, it also triggers a cascade of wound healing events that stimulates osseointegration, a biological process improving implant stability through bone remodelling.

Insufficient primary stability leads to excessive interfacial micromotion following surgery [37, 38], which may imply higher occurrence of migration [39] and of implant failure. Early postoperative migration was suggested to be correlated with long-term loosening after around 8 years [40], emphasising a crucial role of primary stability of cementless implant in the fate of implant survival. Furthermore, the primary stability should not be too high since excessive level of stresses (whose precise amplitude remains to be quantified) may lead to bone necrosis [41, 42].

2.2. Osseointegration and secondary stability

During the post-operative period, bone adapts its structure to the mechanical stresses it undergoes through remodelling phenomena [3], which induces changes of bone properties to accommodate its structure to the presence of the implant. Bone formation relies on complex signalling pathways sensitive to biomechanical stimulation, which remains unclear and is achieved through intramembranous ossification and osteoblasts activation. Bone regeneration after implantation lasts several months during which the spatio-temporal evolution of the bone properties are highly heterogeneous. The main steps of bone regeneration are: (i) the deposition of an extracellular matrix or osteoid tissue, an unmineralised collagen-rich tissue, (ii) mineralisation of the osteoid by hormonal stimulation of local concentration in calcium and phosphates ions to form woven bone (a disordered mineralised tissue) and (iii) remodelling of woven bone to mature bone.

At the macroscopic scale, empirical models have mostly been employed using *ad hoc* assumptions deriving from the Wolff's law [43]. At the nanometre scale, the process of bone formation is affected by local features such as fluid and chemical pathways as well as stress state [44]. Models of bone remodelling should account for the flow channels which provide conduits for fluid flow, enhancing molecular and cellular transport and inducing shear stresses *via* fluid drag at the cell surfaces, an essential condition for cell survival [45, 46]. In particular, fluid flow occurs in the canaliculi [47, 48], which are small channels (diameter between 100 nm and 1 µm [49-51]). Since bone pore walls present a negative surface charge, coupling effects with ions contained in interstitial fluid may appear [52]. Electrical phenomena have been observed in the bone since the 1950s, but its physiological origin is still debated [53, 54]. Methods based on continuum mechanics may not be suited when dealing with fluid transport in nanopores where it is crucial to consider an atomic-level description of the interactions occurring at the interface between the hydroxyapatite and the fluid [55].

Surface effects are likely to play a key role in transport phenomena at the nanoscale in pores with a size not much larger than the molecular size, where hydration and steric effects may induce changes in the fluid properties. One of the main challenges now consists in coupling multi-scale models with temporal bone evolution due to remodelling phenomena [56].

Osseointegration and mature bone in-growth around dental implants allows improving the quantity of bone in contact with the implant as well as bone quality surrounding the implant [57], thus promoting mechanical interlocking [58]. Therefore, the impact of osseointegration phenomena is to strengthen the implant secondary stability, which is a function of healing time. During the early period of healing time (1~3 weeks), a decrease of secondary stability has been described for dental implants, which may be due to osteoclast activity [19].

However, the situation is not so clear regarding orthopaedic implants osseointegration. The term osseointegration indicates a direct and microscopic contact between bone tissue and the implant surface. In orthopedic surgery, there is few evidence that cementless implants are actually osseointegrated. Some authors evidenced a fibrous tissue interface [59] at the BII of orthopedic implants. The reason for hip and knee replacements demonstrating distance osteogenesis is not known but may be related to either the use of certain metals or to the blunt surgery performed with reaming of the marrow cavity and hammering in the implant that shows some micromotion during the first few months after implant placement. However, orthopedic, cementless implants definitely have good clinical outcome, indicating that they show adequate stability probably related to the noticed distance osteogenesis.

During bone healing, low amplitude micromotions stimulate bone remodelling [60], but fibrous tissues may develop instead of an osseointegrated interface in the case of excessive interfacial micromotion following surgery [37], in particular for dental implants. Experimental results showed that micromotion lower than 40~70 μm allows bone tissue in-growth [61]. However, an excessive level (typically above 150 μm) results in the formation of peri-prosthetic fibrous tissue instead of an osseointegrated interface [61-63]. Note that fibrous tissue has a stiffness of around 0.5~2.0 kPa [64], which is several orders of magnitude less rigid than both mature and newly formed bone tissue at the BII. The presence of fibrous tissue therefore affects the load-bearing capacity of the implant and leads to a vicious circle (since micromotions are further enhanced) responsible for implant failures. Moreover, fibrous connective tissue can form on the long term owing to release of wear particles from implant bearing surface [65, 66], in particular in orthopedic surgery.

Resonant frequency analysis (RFA) has become a widely used method to determine secondary stability of dental implant [67]. RFA is a non-invasive technique to assess *in vivo* dental implant stability by measuring the variation in stiffness of the bone-implant system [68, 69], which is presented by an implant stability quotient (ISQ) value. High ISQ values are synonymous to important implant stability [70]. Readers are referred to other reviews [19, 71, 72] for more details on the RFA technique, which is out of scope of the present study.

3. Macroscopic testing of the bone-implant interface

Various types of biomechanical testing employing different loading conditions have been introduced in order to measure the biomechanical properties of the BII. Some authors have considered implants actually used in the clinic (see subsection 3.1) while others have employed custom made implants with a simplified geometry and loading conditions, which allows to work under standardised conditions. Initial mechanical fixation at immediate post-operative period t_0 (Fig. 1a) will be studied in subsection 3.2, including the frictional behaviour of the BII. The evolution of the biomechanical properties of the BII during osseointegration will then be investigated using various approaches in subsection 3.3.

3.1. Using implants employed in the clinic

Many studies in the dental and orthopaedic fields have been carried out using implants employed in clinical practice. Two different testing configurations can be distinguished. The first one consists in an estimation of the micromotion at the BII while the second one consists in realising macroscopic pull-out test.

3.1.1 Micromotion measurement.

An 'excessive' level of micromotion at the BII limits the chances of implant success, which explains why different groups have measured micromotions through the application of cyclic stresses onto the implant. Such approach has been carried out by implant manufacturers to validate the design of new implants [73, 74]. Although the threshold above which osseointegration fails depends on the patient, a micromotion level above 150 µm is commonly accepted to possibly induce implant failure [61-63].

Various studies have evaluated micromotion obtained under physiological loading during patient's daily activities [38], which was often determined through gait analysis by marker clusters and instrumented implants with sensors such as strain gages [75-78]. Various angles were determined for the loading direction relatively to the implant axis, which led to a combination of axial, bending and torsional loading conditions allowing to mimic *in vivo* loading conditions [79].

Advanced image processing techniques such as micro-extensiometry [73] and digital image correlation [80, 81] have been employed to increase the sensitivity of the technique. However, although *post-mortem* studies may be carried out to analyse the BII [82], one important limitation for *in vivo* practices lies in the fact that the BII cannot be directly observed, thus limiting the measurement accuracy. An advanced µCT-based technique was developed to measure relative micromotions between markers located at the implant surface and markers fixed in the surrounding bone, allowing to assess the primary stability of the femoral stem [33]. Linear variable differential transducer (LVDTs) is another technique to measure micromotion at the BII and to evaluate femoral stem primary stability. These devices are

fixed in holes drilled at the bone surface allowing contact with the prosthesis to measure micromotions between the two components at interesting locations [83-87]. However, such methods cannot be implemented in the operative room because of metal artefacts due to metal implants for the µCT-based technique and of the unphysiological aspect of LVDTs.

Micromotion values obtained experimentally have been compared with numerical models. For instance, a 3-D finite element model was developed to predict the interfacial micromotion of cementless knee-tibia prosthesis and to assess the risk of aseptic loosening. The numerical results were compared with experimental measurements under walking and stair climbing loading [31]. Similar approaches have been carried out for femoral stem implants [88-91].

3.1.2 Pull-out tests

The measurement of the maximum pull-out force is another parameter that has been used to estimate the implant stability [90], because the pull-out force is directly related to the implant loosening [92]. Many studies have been carried out using such approach for various types of implants such as hip [93] and knee [92] implants (in cadaveric studies) or dental implant [94] for example. However, a strong limitation of such approach lies in that the crack propagates in an unstable manner at the BII, which prevents investigating the interface mechanical strength.

3.2 Dedicated implant models to measure the initial mechanical fixation

All implants employed in clinical practice have a complex geometry which leads to spatially complex, non-uniform, multiaxial stress fields [95] when the implant is loaded. This heterogeneous stress distribution involving compressive and shear stresses components may influence the results obtained in such configuration [94] and it is therefore difficult to analyse the results in order to estimate a physically meaningful value for the interfacial mechanical strength. This is the reason why dedicated implant models have been developed, since mechanical parameters can be experimentally determined under a controlled and standardized situation, allowing to work under simpler situations. Such implants are considered in this subsection.

The frictional behaviour at the BII provides initial mechanical fixation for implants primary stability. Assessing the friction coefficient is important to understand the behaviour of the BII during and just after surgery and thus to prevent micromotion at the BII, which may cause implant failure. Moreover, the frictional behaviour is an important input parameter to be used in finite-element models [96, 97] in order to model implant surgical procedures.

The most common experimental configuration to measure the friction coefficient is to apply a displacement of the implant perpendicularly to the BII and to induce sliding by moving one domain relatively to the other one in the plane of the interface (see Fig. 2a). Rancourt et al. [98] carried out a seminal work in this domain and evidenced a non-linear friction behavior at the initial stage prior to complete sliding, which corresponds to a non linear variation of the

tangential force as a function of the displacement. The non-linear behavior could be defined by a gradual process – complete stiction, partial stiction and partial sliding, complete sliding – similarly as described in [99]. It was also evidenced that the friction coefficient was independent to the applied normal force [30, 98, 100] and displacement rate [98], but depends on properties of bone tissue surrounding the implant [100] and on the properties of the implant surface [30, 98, 100]. However, further work is needed in order to investigate the dependence of the non linear variation of the tangential force as a function of the displacement (i.e. for low values of displacement).

Biemond et al. [58] considered an alternative experimental configuration by placing a roller on top of the implant, which is used to apply a load perpendicularly to the implant surface (see Fig. 2b). Another testing configuration was developed by Grant *et al.* [101], who considered the application of the normal force using a constant weight (see Fig. 2c), which may not occur using testing machine under load-controled regimes due to possible issues related to the sensitivity of force feedback system [73]. To the best of authors' knowledge, no study coupled roller and weight-load to minimise errors in friction coefficient measurement, which results from variation of normal force and mismatch between the loading direction and the normal direction of contact surface.

Other studies [27, 92] implemented realistic configurations to investigate the dependence of the maximum pull-out force after fully inserting implants into bone cavities. For instance, cylindrical shaped implants with various surface roughness were inserted into bone cavities slightly smaller than the implant size (the difference between the diameters of the implant and of the cavity is called the interference fit). The pull-out forces was then measured, thus allowing to relate the interference fit and implant primary stability [27]. The results demonstrated that larger interference fit leads to higher values of the pull-out force. While non osseointegrated implants (i.e. in the absence of any healing) with rough surfaces are expected to lead to higher pull-out force due to higher friction, an opposite behaviour was obtained in [27], which could stem from bone damage, wear and bone debris generated during the insertion and acting as lubrication. The impact of the interference fit can also be studied with finite element models as in [102, 103] where the results were compared with experimental data.

Another testing configuration was developed by Bishop at al [104-106] in a series of papers in order to model the press-fit configuration (see Fig. 2d) and take into account the effect of the interference fit. They considered two parallelepiped specimens for the bone sample and for the implant. This testing configuration allows the measurement of radial loading, which is important to understand bone deformation and damage during press-fitting. Two methods were developed – force and displacement controlled modes – to model the primary stability of press-fitted implants. The pull-out force was used as a surrogate of the implant primary stability in order to compare the effect of various loading conditions and implant surface properties on primary stability. Bone damage was characterised by analysing the structural change of the bone surface. In the tested configuration, the implant primary stability was shown to depend on the press-fit related stress and to be independent of the roughness of the implant surface and of bone density [105, 106]. Moreover, the friction coefficient was found

to be related to normal stress for a porous-surface implant, especially for high stress level [104].

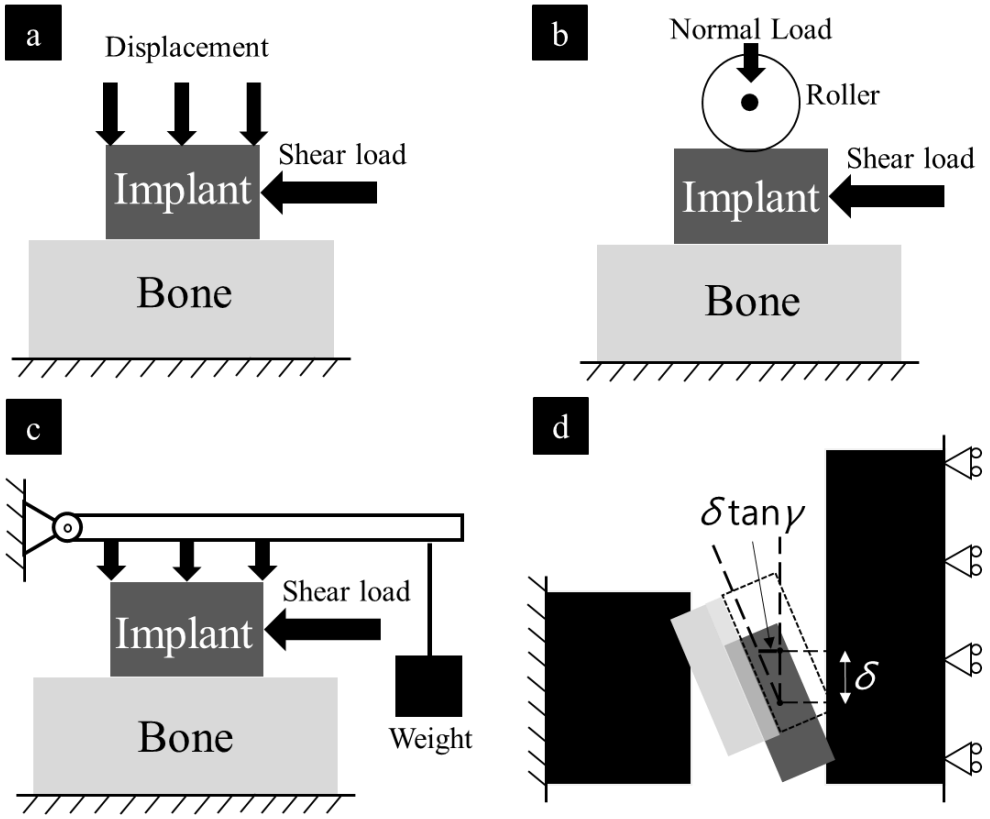

Figure 2 : Schematic description of different experimental configurations dedicated to the measurement of the frictional behaviour of the bone-implant interface. (a) Applied normal pressure, (b) applied normal load with a loading direction perpendicular to bone-implant interface, (c) constant normal pressure applied using a weight and (d) simplified press-fit test accounting for interference fit.

Table 1 summarises the results found in the literature for different values of the friction coefficients of the BII with various types of biomaterials, surface properties, testing configurations and normal forces. Based on the documented values in Table 1, two conclusions can be made. First, bovine trabecular bone with higher porosity than bovine cortical bone leads to higher friction coefficient [107]. Second, higher surface roughness leads to higher value of friction coefficient [101, 104]. In particular, the values of the friction coefficient obtained in human cortical bone [58] seem higher than the values obtained in human trabecular bone [101]. However, the results in cortical bone [58] were obtained at 37 °C in water, which is not the case of those obtained in trabecular bone. Hydration state is likely to have a significant effect on the frictional behaviour of the BII. Moreover, the surface roughness of Ti implant used in [58] was not provided. Most measurements were realised with relatively low normal stresses (< 1 MPa), thus leading to a weak dependence of the frictional behaviour on the normal force.

Table 1: Summary of the results found in the literature for the friction coefficients of implants with various types of biomaterials, surface properties, testing configurations and normal forces.

	implant materials		Implant surface characteristics		testing condition		testing configuration	normal stress/force (MPa)	Friction coefficient	Ref.
	Materials	Surface treatment	Roughness Ra (µm)	Porosity (%)	Temp.	Ambience				
Human trabecular bone	Titanium	Polish	0.11	-	Room temp.	Air	cyclic dynamic sliding in sinusoidal pattern	0.25, 0.5 and 1	0.37 ± 0.02	[101]
		Al2O3-blast	11.00						0.48 ± 0.06	
		Plasma-spray	19.00						0.45 ± 0.03	
		Beaded porous	32.60						0.42 ± 0.01	
Human trabecular bone	Titanium	Polish	0.11	0	Room temp.	Air	Simplified interference fit	Peak magnitudes of 5.6–11.7	0.16 ± 0.05	[104]
		Beaded porous	32.6	45					0.86 ± 0,02	
		Flaked porous	133	63					1.08 ± 0.04	
Human trabecular bone	-	Beaded porous	-	-	Room temp.	Air	Sliding	0.1, 0.15 and 0.25	0.68 ± 0.10	[100]
	Co-Cr alloy	Nonplanar mesh							0.75 ± 0.12	
		Cast mesh type I							0.66 ± 0.09	
		Cast mesh type II							0.94 ± 0.14	
Human trabecular bone	Titanium	Beaded porous	-	-	Room temp.	Air	Sliding	0.1-0.4	0.53 ± 0.07	[98]
		Fiber meshed							0.47 ± 0.03	
	Stainless steel	Smooth							0.30 ± 0.02	
Human trabecular	Titanium	Fiber meshed	-	35-45	Room temp.	Air	Sliding	0.1, 0.15 and 0.25	0.63 ± 0.01	[30]

bone		Beaded porous (Zimmer)		40-70					0.62 ± 0.02	
		Beaded porous (Vitallium)		30-40					0.53 ± 0.02	
	Stainless steel	Smooth		0					0.43 ± 0.01	
Bovine trabecular bone	Porous tantalum	Net-shape formed	-	-	Room temp.	Air	Sliding	-	0.98 ± 0.17	[107]
		Electron-discharge-machine formed							0.88 ± 0.09	
Bovine cortical bone		Net-shape formed							0.82 ± 0.15	
		Electron-discharge-machine formed							0.74 ± 0.07	
Bovine trabecular bone	-	OsteoAnchor	-	-	Room temp.	Air	Unidirectional rotation	0.57 and 0.85	1.04 ± 0.18	[73]
	Tantalum	Porous							0.95 ± 0.05	
	Titanium	Plasma-spray							0.55 ± 0.05	
Human cortical bone	Ti6Al4V	E-beam wave pattern	-	-	37 °C	Water	Sliding	40 N	0.68 ± 0.04	[58]
		E-beam cubic pattern							0.63 ± 0.03	
	Titanium	Plasma-spray							0.64 ±0.04	
		Sandblasted							0.49 ± 0.06	

3.3 Variation of the biomechanical properties of bone-implant interface during healing

3.3.1 Shear and tensile test

The properties of the BII during healing have been measured using push-out and pull-out tests (see Fig. 3a-b). An example can be found in Castellani *et al.* [108] and Tschegg *et al.* [109] who measured the stiffness and the energy necessary to detach the implant, which was given by the area under the load-displacement curves [108, 109]. However, the results are highly dependent on crack initiation since the crack propagates in an unstable manner, which prevents retrieving useful information on the effective adhesion energy of the BII. Another experimental pull-out configuration consisted in using cylindrical implants in combination with an anchoring plate (see Fig. 3b) [110]. The anchoring plate was used to isolate the bottom surface of the implant from bone tissue, ensuring that no stress was applied to this bottom surface during the pull-out phase. Another study also considered cylindrical implants under push-out tests [111], where the BII shear modulus was defined by the slope of the stress/strain unloading curve.

Although the pull-out and push-out tests described above may be qualitatively informative on the biomechanical properties of the BII, strong limitations apply such as for example i) misalignment errors [112, 113] and ii) possible migration of the implant within bone tissue during bone healing. Another (and maybe more important) limitation lies in the fact that cracks propagate in an unstable manner at the BII in mode II (which corresponds to the application of a shear stress applied in the plane of the interface and to a crack propagation in the direction of the principle plane of the solicitation), making it difficult to determine the effective adhesion energy of the BII. When the crack propagates in an unstable manner, the only parameter affecting the macroscopic variable is given by crack initiation and it is then impossible to measure the effective adhesion energy due to the instability of the configuration. Therefore, stable mechanical testing configurations are needed to assess the mechanical strength of the BII. Debonding of the interface depends on a coupling of friction and adhesion phenomena at the BII [108, 109]. Implant retention can be generally regarded as a combined result of friction, mechanical interlocking and chemical bonding [114], which makes it difficult to clearly distinguish between the different effects using such testing configuration.

Therefore, tensile tests in the direction perpendicular to implant surface have been developed in order to minimise the effect of mechanical interlocking, thus, involving mostly adhesive fracture (mode I, which corresponds to the application of a tensile stress applied to the interface) between bone and implant [115, 116] (see Fig. 4c). Ronold et al. [22, 114, 117-119] established an animal model involving the use of a flat coin-shaped implant placed onto cortical bone of a rabbit tibia without mechanical fixation. During the healing period, the contact between the coin-shaped implant and bone tissue is restricted to the flat surface thanks to the presence of polytetrafluoroethylene (PTFE). After the animal sacrifice, the implant was subjected to a quasi-static tensile-loading regime and the effects of surface roughness [117], surface treament [119] and healing time [118] on the pull-out force was investigated. The

results are summarised in Table 2. However, similarly as the configurations described in Figs. 3a&b, the crack propagation occurs in an unstable manner [108, 109] because this pull-out test corresponds to an unstable flat-punch configuration [120]. This situation makes it difficult to determine the effective adhesion energy (or the strain energy release rate), which is the only physically meaningful parameter to investigate the bone-implant attachment, because the measured pull-out force depends on the initial contact conditions in particular around the implant surface. These limitations constitute further motivations to develop alternative approaches such as the torque test configurations described below and introduced in [23].

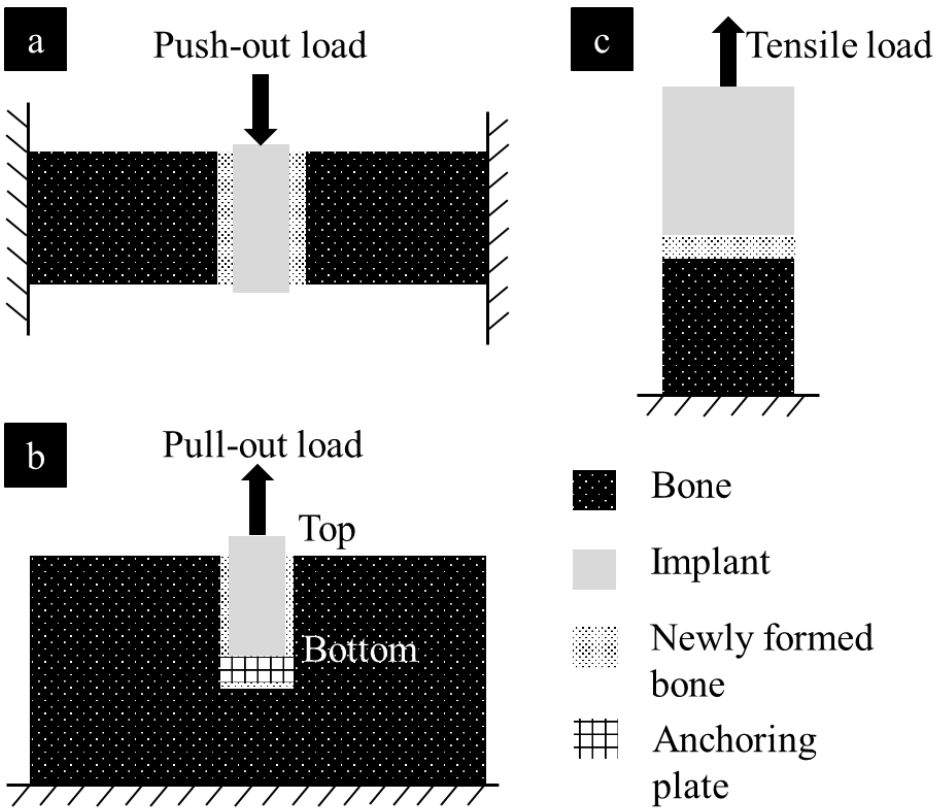

Figure 3: Schematic representation of (a) push-out test, (b) pull-out test and (c) tensile test

3.3.2 Torque test

Torque tests to evaluate osseointegrated implants were initially introduced by Johansson and Albrektsson [23] who started performing manual measurements and then developed automated torque tests [121]. However, from a biomechanical perspective, the implant threading complicate the geometrical configuration, making it challenging to retrieve meaningful parameters from a mechanical point of view. For this reason, a specific implant model having a planar BII and deriving from the seminal papers of Ronold et al. [22, 114, 117-119] was developed by our group. Employing a torque test applied to a coin-shaped implant model constitutes a powerful approach in order to obtain a steady state crack propagation at the BII, as shown in Fig. 4. Moreover, mode III (which corresponds to the

application of a shear stress applied in the plane of the interface and to a crack propagation in the direction perpendicular to the principle plane of the solicitation) is likely to occur *in vivo*, in particular in the case of orthopedic implants, which undergo multiaxial stress field during daily living activity. In this testing configuration, the bone sample is attached to a rotation stage, while a torque sensor is linked to the implant. The crack propagates from the outer part of the planar interface towards the middle of the implant until complete debonding. The phenomena at work at the BII correspond to the coupling of friction and Mode III crack propagation, a situation referred to as stiction [122]. An analytical model taking into account these phenomena was applied, leading to the determination of the effective fracture energy and to the stress intensity factor [123]. The results are summarised in Table 2.

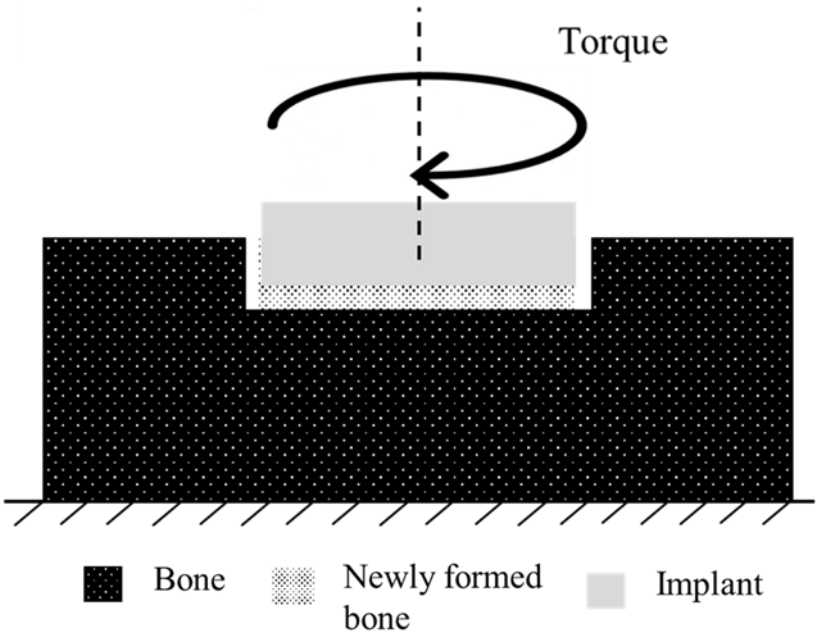

Figure 4: Schematic representation of torque tests with configuration of coin-shaped implant [123].

Table 2: Summary of macroscopic biomechanical properties of BII by tension, shear and torsion tests in literature

Animal mode			Implant			Testing configuration	Biomechanical properties of BII			Ref.
Animal	Contact tissue	Healing period	Material	Surface treatment (particle size)	Surface roughness (R_a, µm)		Stiffness (MPa)	Strength (MPa)	Fracture energy (Nm^{-1})	
New Zealand rabbits	Cortical bone	-	Titanium	TiO_2 blasting	1.43 ± N/A	Coin shaped tension	-	0.11 ± 0.05	-	[114]
		2 weeks		TiO_2 blasting (180–220 µm)	3.37 ± N/A			0.02 ± 0.04		[118]
		4 weeks						0.20 ± 0.18		
		6 weeks						0.45 ± 0.30		
		8 weeks		TiO_2 blasting (22–28 µm)	1.12 ± 0.27			0.11 ± 0.03		[119]
				TiO_2 blasting (180–220 µm)	3.79 ± 1.07			0.84 ± 0.48		
				TiO_2 dual blasting (180–220/22–28 µm)	2.05 ± 0.20			0.16 ± 0.05		
				TiO_2 blasting (180–220 µm)	3.90 ± N/A			0.53 ± 0.30		[117]
				TiO_2 blasting + acid etched (0.01 m HCl)	5.07 ± N/A			0.35 ± 0.18		
				TiO_2 blasting + acid etched (1 m HCl)	11.03 ± N/A			0.09 ± 0.02		
		10 weeks		TiO_2 blasting (22–28 µm)	1.25 ± 0.02			0.66 ± 0.37		[22]
				TiO_2 blasting (180–220 µm)	3.62 ± 0.56			1.78 ± 0.73		
				TiO_2 blasting (270–330 µm)	5.52 ± 0.74			1.53 ± 0.34		
Sprague–Dawley rats	Cortical & trabecular bone	4 weeks	Titanium	-	0.60 ± 0.07	Pull-out shear	-	1.02 ± 0.59	-	[108, 109]
		12 weeks						4.36 ± 0.69		
		24 weeks						2.99 ± 1.62		
		4 weeks	PLGA polymer implant		-			0.98 ± 0.54		
		12 weeks						2.06 ± 0.59		
		24 weeks						1.52 ± 0.64		
		4 weeks	Biodegradable Magnesium alloy		0.76 ± 0.09			2.15 ± 0.59		
		12 weeks						6.75 ± 1.62		
		24 weeks						7.78 ± 1.76		
Pigs	Trabecular bone	3 weeks	Titanium	Grit blasting + high-temperature acid etching	-	Pull-out shear	-	2.60 ± 1.49	-	[110]
				Bio-functionalised P15/HA	-			5.84 ± 2.02		
New	Cortical &	12 weeks	Ti–6Al–4V	Al_2O_3 blasting(500–710 µm)	7.25 ± N/A	Pull-out shear	36.53 ± 19.87	11.78 ± 5.77	-	[111]

Zealand rabbits	trabecular bone		medical grade titanium alloy	Bulged cylindrical pores 100 μm	-		52.04 ± 40.06	8.39 ± 5.00		
				Bulged cylindrical pores 200 μm			53.47 ± 18.86	9.07 ± 2.57		
				Bulged cylindrical pores 300 μm			42.94 ± 10.92	7.85 ± 2.50		
Merino wethers	Cortical bone	4 weeks	Ti–6Al–4V medical grade titanium alloy	Smooth	0.284 ± 0.002	Push-in shear	-	-	-	[124]
		8 weeks						0.75 ± 0.52		
		12 weeks						0.90 ± 1.11		
		4 weeks		Grit-blasted	5.68 ± 0.44			5.89 ± 3.33		
		8 weeks						7.59 ± 3.48		
		12 weeks						10.26 ± 3.11		
		4 weeks		Grit-blasted + HA coated	6.57 ± 0.88			10.02 ± 6.07		
		8 weeks						16.32 ± 5.48		
		12 weeks						20.17 ± 6.52		
		4 weeks		Sintered Ti beads	-			18.58 ± 10.44		
		8 weeks						31.62 ± 5.26		
		12 weeks						34.65 ± 5.33		
		4 weeks		Sintered Ti beads + HA coated	-			17.39 ± 11.33		
		8 weeks						35.31 ± 6.37		
		12 weeks						39.97 ± 5.63		
New Zealand rabbits	Cortical bone	7 weeks	Ti–6Al–4V medical grade titanium alloy	TiO_2 blasting	1.9 ± N/A	Coin shaped torsion	240.00 ± 10.00	1.73 ± 0.08	77.5 ± 7.5	[123]

4. Multiscale characterisation of newly formed bone tissue

As described in section 2, the surgical outcome depends on the evolution of the biomechanical properties of the BII, which are given by the quantity and by the quality of bone tissue around the implant. Therefore, it is important to understand the evolution of the properties of newly formed bone tissue around the implant surface. Histomorphometry is the gold standard to assess osseointegration [125] and allows to measure the BIC ratio. However, histomorphometry cannot be used to retrieve nor bone quality, nor periprosthetic bone biomechanical properties. Moreover, histomorphometry is a destructive technique that cannot be used in clinical practice without having to realize post-mortem experiments. Even if modelling and simulation allow to implement powerful methods taking into account the effect of osseointegration at different scales [31, 126-129], an important advantage of applying multimodality experimental techniques is to be able to retrieve complementary information on the multiscale properties of newly formed bone tissue.

4.1 Nanoindentation and atomic force microscopy

Nanoindentation is one of the reference techniques in order to retrieve the mechanical properties of a medium at the microscale [130, 131]. A rigid indentation tip which has known properties and geometry (such as Berkovich diamond three-sided pyramid probe [6, 132]) presses into a material to retrieve the elastic modulus and hardness by analysing the curves representing the variation of the force as a function of the displacement, in particular at the beginning of the unloading phase using the Oliver and Pharr method [130]. Nanoindentation is an interesting technique to characterise periprosthetic tissue located near the BII because it allows to study the biomechanical properties of newly formed bone tissue. A study compared the elastic modulus and the hardness of newly formed bone tissue around commercially pure titanium (cpTi) implant and titanium-zirconium (TiZr1317) alloy implant after 4 weeks of healing period. The values of the elastic modulus and hardness were higher for the TiZr1317 implant compared to those for the cpTi implant although the difference was not significant [132]. A complementary study has shown that the Young's modulus of newly formed bone tissue also depends on the implant surface treatment since the apparent indentation modulus (respectively the hardness) of periprosthetic bone was around 1.5 (respectively 3) times higher around acid-etched titanium compared to machined titanium [6].

Atomic force microscopy (AFM) is another method used to study the mechanical properties of newly formed bone tissue near the BII and allows to work at a lower scale compared to nanoindentation [64]. The principle of the measurements relies on the analysis of the deflection of a cantilever with a predetermined stiffness. The movement of the cantilever depends on the interactions between its tip and the studied surface and is monitored with a laser system. This set-up results in a force-displacement curve which leads to the elastic modulus and hardness of the material, similarly as in the case of nanoindentation [64, 133].

In a study investigating osseointegration phenomena around titanium implants after 4 weeks of healing time, AFM was used to measure the surface profile. AFM was also used to measure the mechanical response of bone tissue based on the analysis of the curve representing the load as a function of the cantilever tip displacement. The measurements were carried out at

different distances from the implant surface in maxillary and femoral bone tissue. For implants inserted in maxillary bone tissue, the values of the Young's modulus were comprised between 1.04 ± 0.21 MPa and 1.21 ± 0.34 MPa and did not depend on the distance from the implant surface. In contrast, for implants inserted in femoral bone tissue, the values of the Young's modulus were comprised between 0.87 ± 0.25 MPa and 2.24 ± 0.69 MPa and were shown to significantly increase as a function of the distance from the implant surface (between 0-5 µm and 420 µm) [134]. However, the aforementioned values are very low compared to other Young's moduli (of the order of several GPa, see Table 3), and the reasons for such different orders of magnitude remain unclear.

One limitation of the AFM technique lies in that the geometry of the cantilever tip is not precisely known and errors are associated to the estimation of the displacements of the tip in all directions, leading to a lack of precision of the estimation of the elastic modulus and hardness of the investigated tissues. As a consequence, some AFM device may also be used in a nanoindentation mode using well shape-defined diamond tip and adapted load-displacement control [133]. Such configuration was used to study bone tissues in bovine tibia and collagen fibrils in rat tail tendon resulting in values of Young's moduli between 11.8±3.6 and 14.1±5.3 GPa [135] and between 5.0 and 11.5 GPa [136], respectively.

Furthermore, such configuration was implemented to study the BII in an early study evidencing a lower indentation modulus of 6.17 GPa near the BII, which increases with a positive slope of 0.014 GPa/µm in the direction perpendicular to the implant surface until around 150 µm away from the interface. This last result suggests again the existence of a gradient of material properties at the BII, which could be explained by a strongly heterogeneous stress field near the BII, leading to different remodelling conditions [137].

In the aforementioned works, indents were often observed with an optical microscope to check that the indented regions of interest actually correspond to newly formed bone and not to resin or bone defect [6, 137]. However, it was difficult to clearly distinguish between mature and newly formed bone tissue because both types of tissue were interconnected and difficult to clearly distinguish. In order to overcome the aforementioned limitation, we have implemented the implant model described in Fig. 5 in order to create a 200 µm thick bone chamber between mature bone and the implant surface [138-140]. The bone chamber was designed using PTFE layers, as shown in Fig. 5. No bone tissue was present in the bone chamber just after surgery and newly formed bone tissue grows in the bone chamber, which makes it possible to realise nanoindentation measurements in newly formed bone only, and therefore to clearly distinguish mature and newly formed bone tissue. The results showed a significant increase of the apparent indentation modulus as a function of healing time, which may stem from an increase of bone mineralisation [138-140].

The documented values of microscopic biomechanical properties of newly formed tissues around the BII are summarised in Table 3. Non-mineralised fibrous tissue is shown to have a very low indentation modulus, close to that of soft tissue [64]. Cortical bone tissue seems stiffer than trabecular bone tissue [6, 132, 134, 137-140].

However, whether nano-indentation or AFM plays any clinical role remain uncertain [141].

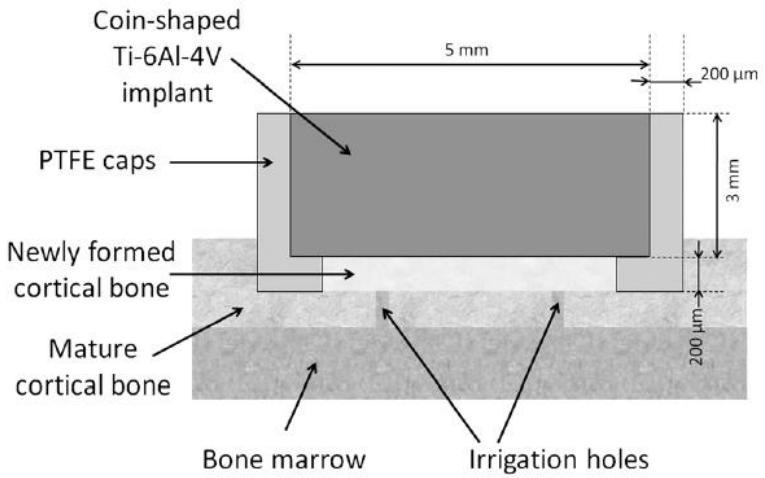

Figure 5 : Schematic representation of the coin-shaped implant model including the bone chamber [138]

Table 3: Summary of the microscopic biomechanical properties of newly formed tissues at BII by indentation-based technique in literature

Animal mode			Implant			Testing configuration	Biomechanical properties of newly formed tissue			Ref.
Animal	Newly formed tissue	Healing period	Material	Surface treatment	Surface roughness (R_a, µm)		Distance from implants (µm)	Young's modulus (Pa)	Hardness (GPa)	
-	Non-mineralised fibrous tissue	-		-	-	AFM	-	0 – 950.5 kPa	-	[64]
						Nanoindentation		0 – 19 kPa		
Sprague–Dawley rats	Mineralised bone tissue	2 weeks	Titanium	Machined surface	0.024 ± 0.005	Nanoindentation	10 ~ 60	7.5 ± 1.07 G	0.18 ± 0.08	[6]
		4 weeks						8.33 ± 1.67 G	0.26 ± 0.03	
		2 weeks		Acid-etching (HCl and H_2SO_4)	0.231 ± 0.051			12.50 ± 2.50 G	0.59 ± 0.15	
		4 weeks						12.50 ± 1.50 G	0.75 ± 0.13	
Sinclair miniswine	Mineralised bone tissue	4 weeks	Titanium	-	-	AFM nanoindentation	<150	7.78 ± 0.47 G	0.189 ± 0.015	[137]
							150 ~ 500	8.61 ± 0.45 G	0.209 ± 0.014	
							500 ~ 800	9.19 ± 0.48 G	0.215 ± 0.015	
							> 800	9.01 ± 0.45 G	0.215 ± 0.014	
Göttingen mini pigs	Mineralised mandibular bone tissue	4 weeks	Commercially pure titanium (cpTi)	Sandblasted acid-etched hydrophilic surface	-	Nanoindentation	cpTi	2.68 ± 0.51 G	0.110 ± 0.017	[132]
			Titanium-zirconium alloy (TiZr1317)				TiZR1317	2.73 ± 0.50 G	0.116 ± 0.017	
New Zealand rabbits	Mineralised cortical bone tissue	4 weeks	Ti–6Al–4V medical grade titanium alloy	TiO_2 blasting	1.9	Nanoindentation	0 ~ 200	15.35 ± 1.81 G	0.643 ± 0.096	[138-140]
		7 weeks						15.85±1.55 G	0.66 ± 0.101	
		13 weeks						17.82±2.10 G	0.668 ± 0.074	

4.2 Quantitative ultrasound

Ultrasound being a mechanical wave, quantitative ultrasound (QUS) techniques are naturally likely to retrieve bone mechanical properties. Another advantage of QUS techniques lies in that ultrasound is non-invasive (ultrasound is even used to stimulate osseointegration [142]), non-radiative and relatively cheap. Note that in the context of osteoporosis assessment, quantitative ultrasound (QUS) is now routinely used clinically to assess bone fragility [143].

It remains difficult to understand the physical phenomena occurring during the interaction between an ultrasonic wave and the BII, due to the complex nature of the BII. Therefore, different finite element models have been implemented because modelling and simulation allows to distinguish the influence of all bone properties (such as compression and shear modulus and mass density) on the ultrasonic response of the BII in a controlled configuration, which is not easy to achieve experimentally because all bone properties vary in parallel. Ultrasound propagation in a dental implant has been modelled using finite element modelling, allowing to derive the dependence of its echographic response on the properties of periprosthetic bone tissue [144, 145]. A limitation of the aforementioned approach lies in that the BII was assumed to be fully bounded and that the roughness was not considered. More recently, a finite element model [146] was developed accounting for the implant roughness as well as for a soft tissue layer corresponding to fibrous tissue. This study showed that the reflection coefficient of an ultrasound wave on the BII depends on the properties of bone tissue located at a distance comprised between 1 and 25 µm from the implant surface, thus opening new path in the investigation of the BII properties. The three aforementioned modelling studies [144-146] showed that QUS techniques around 10 MHz are sensitive to changes of bone properties occurring at a distance lower than around 15 µm from the implant surface.

Experimental models may also be employed to retrieve information on the QUS response of the BII. The echographic response of BII [20] was studied using the coin-shaped implant model described in Fig. 5, which is advantageous because of the planar BII, which allows to work under standardised conditions. The amplitude of the echo of the BII measured at around 15 MHz was shown to decrease as a function of healing time. This result can be explained by the increase of bone quality and quantity around the implant surface, which leads to a decrease of the gap of mechanical properties at the BII during healing.

The same coin shaped implant model has also been used in combination with Micro-Brillouin scattering, a technique consisting of exploiting the coupling of laser and ultrasound in order to retrieve the ultrasonic velocity at the same scale (several micrometres) than the nanoindentation measurements described in the last subsection [19, 139]. The results showed that the ultrasonic velocity at the microscale in newly formed bone tissue and in mature bone tissue were significantly different and equal to around 4930 and 5250 m/s, respectively [139]. Coupling nanoindentation and Micro-Brillouin scattering allowed to retrieve two complementary bone properties (the apparent indentation modulus and the ultrasonic velocity) at the same scale. Comparing the indentation modulus and the ultrasonic velocity allowed to determine that mass density of mature bone tissue is around 13% higher than mass density of

newly formed bone tissue at the scale of several micrometres [139]. This last result can be explained by the increase of mineralisation during bone tissue ageing.

4.3 Other promising approaches

Many authors have investigated the properties of bone tissue in the bulk, but relatively few have focused on periprosthetic tissue, in particular because of the difficulty to simultaneously obtain adapted sample and to carry out complex multimodality experiments. The investigation of the BII at the nano-scale is of particular interest when studying implant anchorage, as bone rupture starts between collagen fibres and the hydroxyapatite crystals [147]. Different techniques have been employed and are described below such as X-ray, neutron and electron-based techniques and spectroscopy.

4.3.1 X-ray based techniques

Optical microscopy techniques are often used to observe biological tissues, but they consist in analysing 2D sections. To improve such analysis, three-dimensional techniques have been developed such as X-ray micro-computed tomography [148, 149], which allows to image woven bone formation at a titanium interface at the microscale [150] for further finite element analysis at microscopic level [151].

X-ray diffraction techniques [152-157] and *small-angle x-ray scattering* (SAXS) [158] have been used to characterise the inorganic structure of bulk bone, like the shape and orientation of hydroxyapatite crystals. Little work has been done using *SAXS* to investigate the periprosthetic bone tissue. The mineral crystals close to the implant surface were found to be preferentially aligned with the implant surface [158]. However, no work has been done on the evolution of this alignment overtime and space during osseointegration.

X-ray diffraction investigates intensity ratios, which indicate the c-axis orientation of biological apatite (BAp) in bone [153, 155-157]. Such technique shows that the BAp crystal c-axis orientation is often parallel to the existing collagen fibres [153]. Note that the orientation of newly formed collagen fibres is approximately parallel to the existing collagen fibres [156]. Furthermore, the BAp crystal preferential alignment follows the local stress distribution as it has been shown in the mandible near the tooth because of mastication forces [153, 155]. Therefore, orientation quantities (intensity ratio of the peak characteristics of the BAp c-axis, tilt angle) appear to be related to diverse bone properties such as the ultrasonic wave velocity [154], Young's modulus [156] and microhardness [159]. The BAp crystal orientation is thus an interesting indicator for mechanical bone properties. Likewise, X-ray diffractometers have been used to study the alignment of the BAp crystals in comparison with the stress distribution and the orientation of grooves on the surface of a hip implant [160] or at the neck of dental implants [161].

Roentgen stereophotogrammetry analysis (RSA), also called radiostereometry, is a radiographic observation technique aiming at obtaining a three-dimensional motion analysis, initiated by Selvik in 1976 [162]. Comparing with ordinary radiography, RSA shows a much higher resolution thanks to the metallic markers, such as small tantalum balls, injected in the bone and on the implant surface that allows analysis of a very small movement [163, 164],

thus, providing a promising non-invasive measurement to assess joint replacement, such as prosthetic fixation, joint kinematics as well as stability of implant [39, 40, 165].

4.3.2 Neutron based techniques

Neutron microcomputed tomography is a promising technique to investigate the BII because of the absence of metal artefacts obtained with X-ray based techniques. A dental implant integrated in a rat tibia has been investigated with both X-rays and neutron tomography at different resolutions [166]. Bone ingrowth was shown to be equivalent for all images except with the neutron images of the lowest resolution. Neutron tomography has then been used in combination with pull-out test [167]. As a result, neutron images allowed to quantify bone growth at the interface without artefacts and the images were analysed to follow the evolution of strains and cracks in the surrounding bone as the implant was pulled-out and until the BII failure.

4.3.3 Electron based techniques

Electron tomography is another promising technique allowing to visualise the three-dimensional structure at a high resolution [168]. Electron tomography was used to investigate in 3D the interface between human bone and a hydroxyapatite implant, which allowed the observation, at the nanometre scale, of hydroxyapatite crystal orientation around the implant surface in comparison with the orientation of crystals in the collagen matrix of bone. Another function of electron tomography is elemental analysis [148], as in [169] which provides elemental mapping of Ca, P, O and Ti at the implant interface. Electron tomography samples can be prepared with the focused ion beam (FIB) method thus producing thin lamella [148, 150].

4.3.4 Spectroscopic approaches

Two spectroscopic methods (Fourier-transform infrared spectroscopy, FTIR and Raman spectroscopy) have been employed to characterise the composition of mature and newly formed bone tissue. These two techniques have been used to study the structural changes in bone tissue depending on the distance to the implant during osseointegration around an artificial composite bone material [170]. FTIR spectroscopy allows to characterise bone mineral and matrix components by comparing the results with a reference spectrum. The components provide information on bone microstructural properties such as mineral content, crystallinity and collagen maturity at the nanometre scale thanks to the combination of FTIR and AFM techniques [171].

On the other hand, Raman spectroscopy provides similar information than FTIR spectroscopy on samples of various types and with easier sample preparation. The drawbacks of Raman spectroscopy compared to FTIR are a lower signal-to-noise ratio and possible fluorescence. In a study carried out in bone tissue, the parameters derived from the analysis of the Raman spectra have been shown to be related to the bone biomechanical properties, and their correlation depends on the animal age [172, 173]. Raman spectroscopy has also been used to study the BII in an *in vivo* study with 3D printed Ti6Al4V implants after 6-month healing in

sheep femora. The Raman analysis was used characterise the molecular composition of both native and newly formed bone tissue at the BII [174].

5. Influence of the implant properties

During bone healing, the evolution of the properties of newly formed bone tissue described in the previous section depends on many factors including the implant stiffness and the implant surface topology, which will be discussed in what follows.

5.1 Implant stiffness

The majority of endosseous implants are made of commercially pure titanium or titanium alloy for oral implants and of titanium alloys, chrome-cobalt molybdenum alloys and stainless steels for orthopedic implants because of their excellent biocompatibility, corrosion resistance and high strength-to-weight ratio [175]. Meanwhile, a common problem, referred to as stress-shielding in the literature, is related to the contrast of density and of stiffness between bone and the implant, which may cause inhomogeneous stress distribution and stress concentration at the vicinity of the implant, thus increasing the risks of implant failure. Stress shielding effects have been shown to be important for orthopaedic implant but less significant around dental implants [176, 177].

A stiffer orthopaedic implant is known to lead to higher level of bone mineral loss in the vicinity of the implant [178]. Similar results have been obtained using finite element studies [179, 180]. Thomas and Cook [113] systematically investigated the effect of elastic modulus of implant on shear stiffness and strength of the BII. The elastic modulus of the implant material covered a large range of variation, from 3 GPa (polymethyl methacrylate, PMMA) to 385 GPa (Al_2O_3). The authors reported no significant effect of the implant stiffness on the mechanical properties of the BII. However, a large range of variation of the results on interface strength and stiffness in each tested group was obtained, which might come from inter-individual variations as well as from variations of the surface roughness that was not controlled. Gottlow et al. [181] demonstrated that implants made of titanium–zirconium alloy (TiZr1317) with lower stiffness and similar surface treatment and implant geometries presented higher removal torque compared to cpTi implants. In order to decrease the effects due to stress-shielding, another approach consists in developing customised porous implants using 3D printing technology [182] or laser power-bed fusion [91]. Other studies attempted to develop Ti-based metallic materials with lower stiffness, improving bone remodelling to enhance mechanical properties of the BII [183-185]. However, the variation of surface composition between implants may also influence the results, which makes it difficult to attribute the difference in terms of osseointegration to stress shielding effects only.

5.2 Implant Surface

Biomaterial surfaces may undergo various modifications affecting their physical, chemical and viscoelastic properties [186] in order to obtain an optimal surface topography, that has been shown to influence osseointegration [5, 187]. Surface roughness not only enhance primary stability, as mentioned in subsection 3.2, but also stimulate bone tissue repair [6,

188]. However, a compromise should be found concerning the roughness level of the implant surface. Wennerberg et al. [141] were the first authors to clearly differentiate between smooth, minimally rough, moderately rough and rough surfaces and to describe a peak in the bone response for moderately rough surfaces. As reviewed in [141], moderately rough (S_a between 1 and 2 µm) surfaces showed stronger bone responses than smooth (S_a <0.5 µm), minimally rough (S_a between 0.5 and 1 µm) and rough (S_a >2 µm) implant surfaces. In another study, the optimal value of S_a (defined by the average height deviation of the surface) optimising osseointegration was shown to be around 3.6-3.9 µm [22, 117]. However, the experiments described in [22, 117] were realised with a simple coin-shaped implant model generating low level of mechanical stresses within bone tissue because of the implant specific macroscopic geometrical configuration without any threading. The roughness should be sufficiently high in order to stimulate bone remodelling but not too high because excessive roughness may create stress concentration and debris damaging bone tissue, thus hampering osseointegration processes.

As indicated in Tables 1-3, most surface topographical analyses were done using the so-called R_a values and were evaluated with stylus instruments, which constitutes a strong limitation because such approach does not provide reliable evaluations of the true surface roughness [141]. Wennerberg and Albrektsson (2000) [189] systematically evaluated three main types of measurement – mechanical contact profilometers, optical profiling instruments, scanning probe microscopes – with their advantages and disadvantages in implant research. Optical profiling instruments, such as interferometry, was suggested to be the most suitable method for assessing surface roughness since it can process measurements of complex geometries and be effective at the micrometer level of resolution which is the clinically relevant one. Anything but 3-D S_a analyses seems of limited interest. Surface roughness analysis must be investigated in relevant areas of the bone anchored parts of the implants and not in irrelevant flat surfaces never in contact with bone tissue [189]. Many studies[22, 108-111, 114, 117-119, 123, 124] documented a height deviation parameter, R_a/S_a, describe surface roughness as shown in Table 2; while, as reviewed in [141] a combination of R_a/S_a, spatial and hybrid parameters (such as *Sdr%* defined in [141]) would be a standard to provide a better surface characterization for modern implants.

6. Conclusion

Understanding the biomechanical behaviour of the BII is a difficult problem because bone is a complex medium, which evolves in time due to remodelling phenomena. The presence of a rough interface complicates the situation by creating complex multiaxial stress around the implant surface. The difficulty also comes from the multifactorial determinants of the problem, given by the implant properties (determined by the implant manufacturer), by the surgical protocol (that is not standardised) and by the patient bone quality and behaviour. The phenomena responsible for implant osseointegration are far from being understood and measuring periprosthetic bone properties remains a challenge.

The ultimate dream of patients and surgeons would be to be able to understand and eventually to predict the implant evolution as a function of the environment, in order to provide a

decision support system that could be designed using for example deep learning based approaches in a patient specific manner. To reach this long-term goal, a better understanding of the biomechanical phenomena is needed, which can be achieved through the coupling of experimental surgery with multimodality measurement approaches providing complementary information on the evolution of periprosthetic bone tissue. In particular, acoustical methods are promising because they may be used to provide information on the bone biomechanical properties non-invasively. However, experimental techniques remain limited to understand the basic phenomena because it is impossible to control all bone properties, which vary in parallel. Therefore, dedicated mechanical models must be developed in parallel to the experiments. These models should in particular account for the adhesive contact at the BII as well as for the roughness of the implant, both in the static and dynamic regimes.

A better understanding of the basic phenomena will lead i) to the development of medical devices aiming at helping the surgeon determining the implant stability during and after surgery and ii) to useful information for the implant manufacturer to improve the quality of their product.

Funding

This project has received funding from the European Research Council (ERC) under the European Union's Horizon 2020 research and innovation program (grant agreement No 682001, project ERC Consolidator Grant 2015 BoneImplant).

References

1. Williams, D.L. and B.M. Isaacson, *The 5 Hallmarks of Biomaterials Success: An Emphasis on Orthopaedics.* Adv Biosci Biotechnol, 2014. **2014**.
2. Gao, X. and I. Sevostianov, *Connection between elastic and electrical properties of cortical bone.* J Biomech, 2016. **49**(5): p. 765-72.
3. Wolff, J., *The Law of Bone Remodeling*. 1986, Berlin: Springer.
4. Winter, W., S.M. Heckmann, and H.P. Weber, *A time-dependent healing function for immediate loaded implants.* J Biomech, 2004. **37**(12): p. 1861-7.
5. Schwartz, Z., E. Nasazky, and B.D. Boyan, *Surface microtopography regulates osteointegration: the role of implant surface microtopography in osteointegration.* Alpha Omegan, 2005. **98**(2): p. 9-19.
6. Butz, F., et al., *Harder and stiffer bone osseointegrated to roughened titanium.* J Dent Res, 2006. **85**(6): p. 560-5.
7. Hansson, S., *Surface roughness parameters as predictors of anchorage strength in bone: a critical analysis.* J Biomech, 2000. **33**(10): p. 1297-303.
8. Brunski, J.B., *In vivo bone response to biomechanical loading at the bone/dental-implant interface.* Adv Dent Res, 1999. **13**: p. 99-119.
9. Dodd, C.A., D.S. Hungerford, and K.A. Krackow, *Total knee arthroplasty fixation. Comparison of the early results of paired cemented versus uncemented porous coated anatomic knee prostheses.* Clin Orthop Relat Res, 1990(260): p. 66-70.
10. Donaldson, A.J., et al., *Bone cement implantation syndrome.* Br J Anaesth, 2009. **102**(1): p. 12-22.
11. Puleo, D.A. and A. Nanci, *Understanding and controlling the bone-implant interface.* Biomaterials, 1999. **20**(23-24): p. 2311-21.
12. Junker, R., et al., *Effects of implant surface coatings and composition on bone integration: a systematic review.* Clin Oral Implants Res, 2009. **20 Suppl 4**: p. 185-206.
13. Skoric, J. and C. Seiler, *Osseointegration: A review of the fundamentals for assuring cementless skeletal fixation.* Orthop Res Rev, 2014. **2014**(default): p. 370-377.
14. Liu, X., P.K. Chu, and C. Ding, *Surface modification of titanium, titanium alloys, and related materials for biomedical applications.* Mater Sci Eng R, 2004. **47**(3): p. 49-121.
15. Lenneras, M., et al., *Oxidized Titanium Implants Enhance Osseointegration via Mechanisms Involving RANK/RANKL/OPG Regulation.* Clin Implant Dent Relat Res, 2015. **17 Suppl 2**: p. e486-500.
16. Omar, O., et al., *Integrin and chemokine receptor gene expression in implant-adherent cells during early osseointegration.* J Mater Sci Mater Med, 2010. **21**(3): p. 969-80.
17. Omar, O.M., et al., *The correlation between gene expression of proinflammatory markers and bone formation during osseointegration with titanium implants.* Biomaterials, 2011. **32**(2): p. 374-86.
18. Palmquist, A., et al., *Titanium oral implants: surface characteristics, interface biology and clinical outcome.* J R Soc Interface, 2010. **7 Suppl 5**: p. S515-27.
19. Mathieu, V., et al., *Biomechanical determinants of the stability of dental implants: influence of the bone-implant interface properties.* J Biomech, 2014. **47**(1): p. 3-13.
20. Mathieu, V., et al., *Influence of healing time on the ultrasonic response of the bone-implant interface.* Ultrasound Med Biol, 2012. **38**(4): p. 611-8.
21. Bolind, P., et al., *A study of 275 retrieved Branemark oral implants.* Int J Periodontics Restorative Dent, 2005. **25**(5): p. 425-37.

22. Ronold, H.J. and J.E. Ellingsen, *Effect of micro-roughness produced by TiO2 blasting--tensile testing of bone attachment by using coin-shaped implants.* Biomaterials, 2002. **23**(21): p. 4211-9.
23. Johansson, C. and T. Albrektsson, *Integration of Screw Implants in the Rabbit: A 1-yr Follow-up of Removal Torque of Titanium Implants.* Int J Oral Maxillofac Implants., 1987. **2**(2): p. 69-15.
24. Branemark, P.-I., *Osseointegrated implants in the treatment of the edentulous jaw. Experience from a 10-year period.* Scand. J. Plast. Reconstr. Surg. Suppl., 1977. **16**: p. 1-132.
25. Liu, S., et al., *Limitations of using micro-computed tomography to predict bone-implant contact and mechanical fixation.* J Microsc, 2012. **245**(1): p. 34-42.
26. Potter, H.G., et al., *Magnetic resonance imaging after total hip arthroplasty: evaluation of periprosthetic soft tissue.* J Bone Joint Surg Am, 2004. **86-A**(9): p. 1947-54.
27. Berahmani, S., et al., *An experimental study to investigate biomechanical aspects of the initial stability of press-fit implants.* J Mech Behav Biomed Mater, 2015. **42**: p. 177-85.
28. Shirazi-Adl, A. and A. Forcione, *Finite element stress analysis of a push-out test. Part II: Free interface with nonlinear friction properties.* J Biomech Eng, 1992. **114**(2): p. 155-61.
29. Shultz, T.R., et al., *Cortical bone viscoelasticity and fixation strength of press-fit femoral stems: finite element model.* J Biomech Eng, 2006. **128**(1): p. 7-12.
30. Shirazi-Adl, A., M. Dammak, and G. Paiement, *Experimental determination of friction characteristics at the trabecular bone/porous-coated metal interface in cementless implants.* J Biomed Mater Res, 1993. **27**(2): p. 167-75.
31. Chong, D.Y., U.N. Hansen, and A.A. Amis, *Analysis of bone-prosthesis interface micromotion for cementless tibial prosthesis fixation and the influence of loading conditions.* J Biomech, 2010. **43**(6): p. 1074-80.
32. ten Broeke, R.H., et al., *Improving peri-prosthetic bone adaptation around cementless hip stems: a clinical and finite element study.* Med Eng Phys, 2014. **36**(3): p. 345-53.
33. Gortchacow, M., et al., *A new technique to measure micromotion distribution around a cementless femoral stem.* J Biomech, 2011. **44**(3): p. 557-60.
34. Suarez, D.R., et al., *Fracture risk and initial fixation of a cementless glenoid implant: the effect of numbers and types of screws.* Proc Inst Mech Eng H, 2013. **227**(10): p. 1058-66.
35. Gaines, R.W., Jr., *The use of pedicle-screw internal fixation for the operative treatment of spinal disorders.* J Bone Joint Surg Am, 2000. **82-A**(10): p. 1458-76.
36. Cuny, C., et al., *The Telegraph nail for proximal humeral fractures: a prospective four-year study.* J Shoulder Elbow Surg, 2008. **17**(4): p. 539-45.
37. Duyck, J., et al., *The influence of micro-motion on the tissue differentiation around immediately loaded cylindrical turned titanium implants.* Arch Oral Biol, 2006. **51**(1): p. 1-9. .
38. Taylor, M., D.S. Barrett, and D. Deffenbaugh, *Influence of loading and activity on the primary stability of cementless tibial trays.* J Orthop Res, 2012. **30**(9): p. 1362-8.
39. Fukuoka, S., K. Yoshida, and Y. Yamano, *Estimation of the migration of tibial components in total knee arthroplasty. A roentgen stereophotogrammetric analysis.* J Bone Joint Surg Br, 2000. **82**(2): p. 222-7.
40. Ryd, L., et al., *Roentgen stereophotogrammetric analysis as a predictor of mechanical loosening of knee prostheses.* J Bone Joint Surg Br, 1995. **77**(3): p. 377-83.

41. Duyck, J., et al., *Histological, histomorphometrical, and radiological evaluation of an experimental implant design with a high insertion torque.* Clin Oral Implants Res, 2010. **21**(8): p. 877-84.
42. Coelho, P.G., et al., *Biomechanical evaluation of endosseous implants at early implantation times: a study in dogs.* J Oral Maxillofac Surg, 2010. **68**(7): p. 1667-75.
43. Cowin, S., *Wolff's law of trabecular architecture at remodeling equilibrium.* J Biomech Eng, 1986. **108**: p. 83-88.
44. Swan, C.C., et al., *Micromechanically based poroelastic modeling of fluid flow in Haversian bone.* J Biomech Eng, 2003. **125**(1): p. 25-37.
45. Checa, S. and P.J. Prendergast, *A mechanobiological model for tissue differentiation that includes angiogenesis: a lattice-based modeling approach.* Ann Biomed Eng, 2009. **37**(1): p. 129-45.
46. Davies, P.F., *Hemodynamic shear stress and the endothelium in cardiovascular pathophysiology.* Nat Clin Pract Cardiovasc Med, 2009. **6**(1): p. 16-26.
47. Sansalone, V., et al., *Interstitial fluid flow within bone canaliculi and electro-chemo-mechanical features of the canalicular milieu: a multi-parametric sensitivity analysis.* Biomech Model Mechanobiol, 2013. **12**(3): p. 533-53.
48. Lemaire, T., et al., *Parametric study of interstitial fluid flow in the bone lacuno-canalicular network.* Comput Methods Biomech Biomed Engin, 2012. **15 Suppl 1**: p. 331-2.
49. Lai, X., et al., *The dependences of osteocyte network on bone compartment, age, and disease.* Bone Res, 2015. **3**.
50. Langer, M., et al., *X-ray phase nanotomography resolves the 3D human bone ultrastructure.* PloS one, 2012. **7**(8): p. e35691.
51. Marotti, G., et al., *Quantitative evaluation on osteocyte canalicular density in human secondary osteons.* Bone, 1995. **16**(1): p. 125-128.
52. Lemaire, T., S. Naili, and A. Remond, *Study of the influence of fibrous pericellular matrix in the cortical interstitial fluid movement with hydroelectrochemical effects.* J Biomech Eng, 2008. **130**(1): p. 011001.
53. Mori, S., et al., *Ultrasonically-induced electrical potentials in demineralized bovine cortical bone.* AIP Adv, 2018. **8**(4): p. 045007.
54. Matsukawa, M. and S. Matsukawa, *Study on Ultrasound Irradiation Induction of Electrical Potentials in Bone.* J Orthop Trauma, 2017. **31**(7): p. S4.
55. Lemaire, T., et al., *Water in hydroxyapatite nanopores: Possible implications for interstitial bone fluid flow.* J Biomech, 2015. **48**(12): p. 3066-71.
56. Martin, M., et al., *A thermodynamically consistent model of bone rotary remodeling: a 2D study.* Comput Methods Biomech Biomed Engin, 2017. **20**(sup1): p. 127-128.
57. Geesink, R.G., K. de Groot, and C.P. KLEIN, *Chemical implant fixation using hydroxyl-apatite coatings: the development of a human total hip prosthesis for chemical fixation to bone using hydroxyl-apatite coatings on titanium substrates.* Clinical Orthopaedics and Related Research®, 1987. **225**: p. 147-170.
58. Biemond, J.E., et al., *Frictional and bone ingrowth properties of engineered surface topographies produced by electron beam technology.* Arch Orthop Trauma Surg, 2011. **131**(5): p. 711-8.
59. Shah, F.A., P. Thomsen, and A. Palmquist, *Osseointegration and current interpretations of the bone-implant interface.* Acta Biomater, 2019. **84**: p. 1-15.
60. Mori, S. and D.B. Burr, *Increased intracortical remodeling following fatigue damage.* Bone, 1993. **14**(2): p. 103-9.

61. Bragdon, C.R., et al., *Differences in stiffness of the interface between a cementless porous implant and cancellous bone in vivo in dogs due to varying amounts of implant motion.* J Arthroplasty, 1996. **11**(8): p. 945-51.
62. Pilliar, R.M., J.M. Lee, and C. Maniatopoulos, *Observations on the effect of movement on bone ingrowth into porous-surfaced implants.* Clin Orthop Relat Res, 1986(208): p. 108-13.
63. Engh, C.A., et al., *Quantification of implant micromotion, strain shielding, and bone resorption with porous-coated anatomic medullary locking femoral prostheses.* Clin Orthop Relat Res, 1992(285): p. 13-29.
64. Moerman, A., et al., *Structural and mechanical characterisation of the peri-prosthetic tissue surrounding loosened hip prostheses. An explorative study.* J Mech Behav Biomed Mater, 2016. **62**: p. 456-467.
65. Haynes, D.R., et al., *The differences in toxicity and release of bone-resorbing mediators induced by titanium and cobalt-chromium-alloy wear particles.* J Bone Joint Surg Am, 1993. **75**(6): p. 825-34.
66. Moreschini, O., et al., *Markers of connective tissue activation in aseptic hip prosthetic loosening.* J Arthroplasty, 1997. **12**(6): p. 695-703.
67. Meredith, N., D. Alleyne, and P. Cawley, *Quantitative determination of the stability of the implant‐tissue interface using resonance frequency analysis.* Clinical oral implants research, 1996. **7**(3): p. 261-267.
68. Friberg, B., et al., *Stability measurements of one-stage Brånemark implants during healing in mandibles: a clinical resonance frequency analysis study.* International journal of oral and maxillofacial surgery, 1999. **28**(4): p. 266-272.
69. Barewal, R.M., et al., *Resonance frequency measurement of implant stability in vivo on implants with a sandblasted and acid-etched surface.* International Journal of Oral & Maxillofacial Implants, 2003. **18**(5).
70. Valderrama, P., et al., *Evaluation of two different resonance frequency devices to detect implant stability: a clinical trial.* Journal of periodontology, 2007. **78**(2): p. 262-272.
71. Lages, F.S., D.W. Douglas-de Oliveira, and F.O. Costa, *Relationship between implant stability measurements obtained by insertion torque and resonance frequency analysis: A systematic review.* Clin Implant Dent Relat Res, 2018. **20**(1): p. 26-33.
72. Zanetti, E.M., et al., *Clinical Assessment of Dental Implant Stability During Follow-Up: What Is Actually Measured, and Perspectives.* Biosensors (Basel), 2018. **8**(3).
73. Harrison, N., et al., *Micromotion and friction evaluation of a novel surface architecture for improved primary fixation of cementless orthopaedic implants.* J Mech Behav Biomed Mater, 2013. **21**: p. 37-46.
74. Abdul-Kadir, M.R., et al., *Finite element modelling of primary hip stem stability: the effect of interference fit.* J Biomech, 2008. **41**(3): p. 587-94.
75. Bergmann, G., et al., *Hip contact forces and gait patterns from routine activities.* J Biomech, 2001. **34**(7): p. 859-71.
76. Ledet, E.H., et al., *Implantable sensor technology: from research to clinical practice.* J Am Acad Orthop Surg, 2012. **20**(6): p. 383-92.
77. Kutzner, I., et al., *Loading of the knee joint during activities of daily living measured in vivo in five subjects.* J Biomech, 2010. **43**(11): p. 2164-73.
78. Nikooyan, A.A., et al., *Validation of the Delft Shoulder and Elbow Model using in-vivo glenohumeral joint contact forces.* J Biomech, 2010. **43**(15): p. 3007-14.
79. Bishop, N.E., et al., *Biomechanics of short hip endoprostheses--the risk of bone failure increases with decreasing implant size.* Clin Biomech (Bristol, Avon), 2010. **25**(7): p. 666-74.

80. Nadorf, J., et al., *Tibial revision knee arthroplasty with metaphyseal sleeves: The effect of stems on implant fixation and bone flexibility.* PLoS One, 2017. **12**(5): p. e0177285.
81. Tijou, A., et al., *Monitoring cementless femoral stem insertion by impact analyses: an in vitro study.* J Mech Behav Biomed Mater, submitted.
82. Bolind, P., et al., *A study of 275 retrieved Brånemark oral implants.* International Journal of Periodontics & Restorative Dentistry, 2005. **25**(5).
83. Enoksen, C.H., et al., *Load transfer in the proximal femur and primary stability of a cemented and uncemented femoral stem: An experimental study on cadaver femurs.* Proc Inst Mech Eng H, 2017. **231**(12): p. 1195-1203.
84. Baleani, M., L. Cristofolini, and A. Toni, *Initial stability of a new hybrid fixation hip stem: experimental measurement of implant-bone micromotion under torsional load in comparison with cemented and cementless stems.* J Biomed Mater Res, 2000. **50**(4): p. 605-15.
85. Cristofolini, L., E. Varini, and M. Viceconti, *In-vitro method for assessing femoral implant-bone micromotions in resurfacing hip implants under different loading conditions.* Proc Inst Mech Eng H, 2007. **221**(8): p. 943-50.
86. Bieger, R., et al., *Primary stability and strain distribution of cementless hip stems as a function of implant design.* Clin Biomech (Bristol, Avon), 2012. **27**(2): p. 158-64.
87. Bieger, R., et al., *Biomechanics of a short stem: In vitro primary stability and stress shielding of a conservative cementless hip stem.* J Orthop Res, 2013. **31**(8): p. 1180-6.
88. Fehring, K.A., et al., *Initial stability of press-fit acetabular components under rotational forces.* J Arthroplasty, 2014. **29**(5): p. 1038-42.
89. Amirouche, F., et al., *Primary cup stability in THA with augmentation of acetabular defect. A comparison of healthy and osteoporotic bone.* Orthop Traumatol Surg Res, 2015. **101**(6): p. 667-73.
90. Amirouche, F., et al., *Factors influencing initial cup stability in total hip arthroplasty.* Clin Biomech (Bristol, Avon), 2014. **29**(10): p. 1177-85.
91. Jette, B., et al., *Development and in vitro validation of a simplified numerical model for the design of a biomimetic femoral stem.* J Mech Behav Biomed Mater, 2018. **77**: p. 539-550.
92. Berahmani, S., et al., *The effect of surface morphology on the primary fixation strength of uncemented femoral knee prosthesis: a cadaveric study.* J Arthroplasty, 2015. **30**(2): p. 300-7.
93. Michel, A., et al., *Assessing the Acetabular Cup Implant Primary Stability by Impact Analyses: A Cadaveric Study.* PLoS One, 2017. **11**(11): p. e0166778.
94. Branemark, R., et al., *Biomechanical characterization of osseointegration: an experimental in vivo investigation in the beagle dog.* J Orthop Res, 1998. **16**(1): p. 61-9.
95. Shirazi-Adl, A., *Finite element stress analysis of a push-out test. Part 1: Fixed interface using stress compatible elements.* J Biomech Eng, 1992. **114**(1): p. 111-8.
96. Nguyen, V.H., et al., *Influence of anisotropic bone properties on the biomechanical behavior of the acetabular cup implant: a multiscale finite element study.* Comput Methods Biomech Biomed Engin, 2017. **20**(12): p. 1312-1325.
97. Raffa, M.L., et al., *Dependence of the primary stability of acetabular cup implants on its biomechanical environment.* Biomech Model Mechanobiol, submitted.
98. Rancourt, D., et al., *Friction properties of the interface between porous-surfaced metals and tibial cancellous bone.* J Biomed Mater Res, 1990. **24**(11): p. 1503-19.
99. Jäger, J., *Axi-symmetric bodies of equal material in contact under torsion or shift.* Arch Appl Mech, 1995. **65**(7): p. 478-487.

100. Dammak, M., et al., *Friction properties at the bone-metal interface: comparison of four different porous metal surfaces.* J Biomed Mater Res, 1997. **35**(3): p. 329-36.
101. Grant, J.A., et al., *Artificial composite bone as a model of human trabecular bone: the implant-bone interface.* J Biomech, 2007. **40**(5): p. 1158-64.
102. Spears, I.R., et al., *The effect of interfacial parameters on cup-bone relative micromotions. A finite element investigation.* J Biomech, 2001. **34**(1): p. 113-20.
103. Michel, A., et al., *Finite element model of the impaction of a press-fitted acetabular cup.* Med Biol Eng Comput, 2017. **55**(5): p. 781-791.
104. Damm, N.B., M.M. Morlock, and N.E. Bishop, *Friction coefficient and effective interference at the implant-bone interface.* J Biomech, 2015. **48**(12): p. 3517-21.
105. Bishop, N.E., et al., *The influence of bone damage on press-fit mechanics.* J Biomech, 2014. **47**(6): p. 1472-8.
106. Damm, N.B., M.M. Morlock, and N.E. Bishop, *Influence of trabecular bone quality and implantation direction on press-fit mechanics.* J Orthop Res, 2017. **35**(2): p. 224-233.
107. Zhang, Y., et al., *Interfacial frictional behavior: cancellous bone, cortical bone, and a novel porous tantalum biomaterial.* J Musculoskelet Res, 1999. **3**(04): p. 245-251.
108. Castellani, C., et al., *Bone-implant interface strength and osseointegration: Biodegradable magnesium alloy versus standard titanium control.* Acta Biomater, 2011. **7**(1): p. 432-40.
109. Tschegg, E.K., et al., *Characterization methods of bone-implant-interfaces of bioresorbable and titanium implants by fracture mechanical means.* J Mech Behav Biomed Mater, 2011. **4**(5): p. 766-75.
110. Nonhoff, J., et al., *Establishment of a new pull-out strength testing method to quantify early osseointegration-An experimental pilot study.* J Craniomaxillofac Surg, 2015. **43**(10): p. 1966-73.
111. Muller, M., et al., *Bone-implant interface shear modulus and ultimate stress in a transcortical rabbit model of open-pore Ti6Al4V implants.* J Biomech, 2006. **39**(11): p. 2123-32.
112. Nakamura, T., et al., *A new glass-ceramic for bone replacement: evaluation of its bonding to bone tissue.* J Biomed Mater Res, 1985. **19**(6): p. 685-98.
113. Thomas, K.A. and S.D. Cook, *An evaluation of variables influencing implant fixation by direct bone apposition.* J Biomed Mater Res, 1985. **19**(8): p. 875-901.
114. Ronold, H.J. and J.E. Ellingsen, *The use of a coin shaped implant for direct in situ measurement of attachment strength for osseointegrating biomaterial surfaces.* Biomaterials, 2002. **23**(10): p. 2201-9.
115. Gross, U., et al., *The ultrastructure of the interface between a glass ceramic and bone.* J Biomed Mater Res, 1981. **15**(3): p. 291-305.
116. Coelho, P.G., et al., *Enhanced Bone Bonding to Nanotextured Implant Surfaces at a Short Healing Period: A Biomechanical Tensile Testing in the Rat Femur.* Implant Dent, 2016. **25**(3): p. 322-7.
117. Ronold, H.J., S.P. Lyngstadaas, and J.E. Ellingsen, *Analysing the optimal value for titanium implant roughness in bone attachment using a tensile test.* Biomaterials, 2003. **24**(25): p. 4559-64.
118. Ronold, H.J., J.E. Ellingsen, and S.P. Lyngstadaas, *Tensile force testing of optimized coin-shaped titanium implant attachment kinetics in the rabbit tibiae.* J Mater Sci Mater Med, 2003. **14**(10): p. 843-9.
119. Ronold, H.J., S.P. Lyngstadaas, and J.E. Ellingsen, *A study on the effect of dual blasting with TiO2 on titanium implant surfaces on functional attachment in bone.* J Biomed Mater Res A, 2003. **67**(2): p. 524-30.

120. Maugis, D., *Frictionless Elastic Contact*, in *Contact adhesion and rupture of elastic solids*. 2000, Springer. p. 236.
121. Johansson, C.B., R. Jimbo, and P. Stefenson, *Ex vivo and in vivo biomechanical test of implant attachment to various materials: introduction of a new user‐friendly removal torque equipment.* Clinical implant dentistry and related research, 2012. **14**(4): p. 603-611.
122. Chateauminois, A., C. Fretigny, and L. Olanier, *Friction and shear fracture of an adhesive contact under torsion.* Phys Rev E Stat Nonlin Soft Matter Phys, 2010. **81**(2 Pt 2): p. 026106.
123. Mathieu, V., et al., *Mode III cleavage of a coin-shaped titanium implant in bone: effect of friction and crack propagation.* J Mech Behav Biomed Mater, 2012. **8**: p. 194-203.
124. Svehla, M., et al., *Morphometric and mechanical evaluation of titanium implant integration: comparison of five surface structures.* J Biomed Mater Res, 2000. **51**(1): p. 15-22.
125. Franchi, M., et al., *Influence of different implant surfaces on peri-implant osteogenesis: histomorphometric analysis in sheep.* J Periodontol, 2007. **78**(5): p. 879-88.
126. Mukherjee, K. and S. Gupta, *Bone ingrowth around porous-coated acetabular implant: a three-dimensional finite element study using mechanoregulatory algorithm.* Biomech Model Mechanobiol, 2016. **15**(2): p. 389-403.
127. Ascenzi, M.G., et al., *Individual-specific multi-scale finite element simulation of cortical bone of human proximal femur.* J Comput Phys, 2013. **244**: p. 298-311.
128. Nackenhorst, U. and C. Lenz, *Biomechanics of bones on various length scales.* PAMM Proc Appl Math Mech, 2005. **5**: p. 31-34.
129. Nackenhorst, U., *Computational methods for studies on the biomechanics of bones* Found Civ Environ Eng, 2006. **7**: p. 251-271.
130. Abdel-Wahab, A. and V. Silberschmidt, *Plastic behaviour of microstructural constituents of cortical bone tissue: a nanoindentation study.* Int J Exp Comput Biomech, 2013. **2**(2): p. 136-157.
131. Demiral, M., A. Abdel-Wahab, and V. Silberschmidt, *A numerical study on indentation properties of cortical bone tissue: influence of anisotropy.* Acta Bioeng Biomech, 2015. **17**(2): p. 3-14.
132. Anchieta, R.B., et al., *Mechanical property assessment of bone healing around a titanium-zirconium alloy dental implant.* Clin Implant Dent Relat Res, 2014. **16**(6): p. 913-9.
133. Jandt, K.D., *Atomic force microscopy of biomaterials surfaces and interfaces.* Surf Sci, 2001. **491**: p. 303-332.
134. Clark, P.A., et al., *Nanoscale characterization of bone–implant interface and biomechanical modulation of bone ingrowth.* Mater Sci Eng C Mater Biol Appl, 2007. **27**(3): p. 382-393.
135. Tai, K., et al., *Nanoscale heterogeneity promotes energy dissipation in bone.* Nat Mater, 2007. **6**(6): p. 454-62.
136. Wenger, M.P., et al., *Mechanical properties of collagen fibrils.* Biophys J, 2007. **93**(4): p. 1255-63.
137. Chang, M.C., et al., *Elasticity of alveolar bone near dental implant-bone interfaces after one month's healing.* J Biomech, 2003. **36**(8): p. 1209-14.
138. Vayron, R., et al., *Nanoindentation measurements of biomechanical properties in mature and newly formed bone tissue surrounding an implant.* J Biomech Eng, 2012. **134**(2): p. 021007.

139. Vayron, R., et al., *Evolution of bone biomechanical properties at the micrometer scale around titanium implant as a function of healing time.* Phys Med Biol, 2014. **59**(6): p. 1389-406.
140. Vayron, R., et al., *Variation of biomechanical properties of newly formed bone tissue determined by nanoindentation as a function of healing time.* Comput Methods Biomech Biomed Engin, 2011. **14**(sup1): p. 139-140.
141. Wennerberg, A. and T. Albrektsson, *Effects of titanium surface topography on bone integration: a systematic review.* Clin Oral Impl Res 2009. **20**(suppl 4): p. S172-184.
142. Li, L., et al., *Ultrasound: A potential technique to improve osseointegration of dental implants.* Med Hypotheses, 2008. **71**(4): p. 568-71.
143. Gluer, C.C. and R. Barkmann, *Quantitative ultrasound: use in the detection of fractures and in the assessment of bone composition.* Curr Osteoporos Rep, 2003. **1**(3): p. 98-104.
144. Vayron, R., et al., *Assessment of the biomechanical stability of a dental implant with quantitative ultrasound: A three-dimensional finite element study.* J Acoust Soc Am, 2016. **139**(2): p. 773-80.
145. Vayron, R., et al., *Finite element simulation of ultrasonic wave propagation in a dental implant for biomechanical stability assessment.* Biomech Model Mechanobiol, 2015. **14**(5): p. 1021-32.
146. Heriveaux, Y., V.H. Nguyen, and G. Haiat, *Reflection of an ultrasonic wave on the bone-implant interface: A numerical study of the effect of the multiscale roughness.* J Acoust Soc Am, 2018. **144**(1): p. 488.
147. Zahn, D. and P. Duchstein, *Multi-Scale Modelling of Deformation and Fracture in a Biomimetic Apatite-Protein Composite: Molecular-Scale Processes Lead to Resilience at the mum-Scale.* PLoS One, 2016. **11**(6): p. e0157241.
148. Palmquist, A., *A multiscale analytical approach to evaluate osseointegration.* J Mater Sci Mater Med, 2018. **29**(5): p. 60.
149. Du, J., et al., *Biomechanics and strain mapping in bone as related to immediately-loaded dental implants.* Journal of biomechanics, 2015. **48**(12): p. 3486-3494.
150. Thorfve, A., A. Palmquist, and K. Grandfield, *Three-dimensional analytical techniques for evaluation of osseointegrated titanium implants.* Mater Sci Technol, 2015. **31**(2).
151. Mao, Q., et al., *Voxel-based Micro-finite Element Analysis of Dental Implants in a Human Cadaveric Mandible: Tissue Modulus Assignment and Sensitivity Analyses.* Journal of the Mechanical Behavior of Biomedical Materials, 2019.
152. Hirata, K., et al., *Fabrication of oriented hydroxyapatite film by RF magnetron sputtering.* AIP Adv, 2017. **7**(085219).
153. Nakano, T., et al., *Unique alignment and texture of biological apatite crystallites in typical calcified tissues analyzed by microbeam X-ray diffractometer system.* Bone, 2002. **31**(4): p. 479-87.
154. Yamato, Y., et al., *Correlation between hydroxyapatite crystallite orientation and ultrasonic wave velocities in bovine cortical bone.* Calcif Tissue Int, 2008. **82**(2): p. 162-9.
155. Ishimoto, T., et al., *Changes in bone microstructure and toughness during the healing process of long bones.* J Phys Conf Ser, 2009. **165**.
156. Ishimoto, T., et al., *Degree of biological apatite c-axis orientation rather than bone mineral density controls mechanical function in bone regenerated using recombinant bone morphogenetic protein-2.* J Bone Miner Res, 2013. **28**(5): p. 1170-9.

157. Matsugaki, A., et al., *Quantitative regulation of bone-mimetic, oriented collagen/apatite matrix structure depends on the degree of osteoblast alignment on oriented collagen substrates.* J Biomed Mater Res A, 2015. **103**(2): p. 489-99.
158. Bunger, M.H., et al., *Bone nanostructure near titanium and porous tantalum implants studied by scanning small angle x-ray scattering.* Eur Cell Mater, 2006. **12**: p. 81-91.
159. Ziv, V., H.D. Wagner, and S. Weiner, *Microstructure-microhardness relations in parallel-fibered and lamellar bone.* Bone, 1996. **18**(5): p. 417-28.
160. Noyama, Y., et al., *Quantity and quality of regenerated bone in grooves aligned at different angles from the implant surface.* Mater Sci Forum, 2010.
161. Kuroshima, S., et al., *Optimally oriented grooves on dental implants improve bone quality around implants under repetitive mechanical loading.* Acta Biomater, 2017. **48**: p. 433-444.
162. Selvik, G., *Roentgen stereophotogrammetry: a method for the study of the kinematics of the skeletal system.* Acta Orthopaedica Scandinavica, 1989. **60**(sup232): p. 1-51.
163. Kärrholm, J., *Roentgen stereophotogrammetry: review of orthopedic applications.* Acta Orthopaedica Scandinavica, 1989. **60**(4): p. 491-503.
164. Valstar, E.R., et al., *Guidelines for standardization of radiostereometry (RSA) of implants.* Acta orthopaedica, 2005. **76**(4): p. 563-572.
165. Soballe, K., et al., *Migration of hydroxyapatite coated femoral prostheses. A Roentgen Stereophotogrammetric study.* The Journal of bone and joint surgery. British volume, 1993. **75**(5): p. 681-687.
166. Isaksson, H., et al., *Neutron tomographic imaging of bone-implant interface: Comparison with X-ray tomography.* Bone, 2017. **103**: p. 295-301.
167. Le Cann, S., et al., *Characterization of the bone-metal implant interface by Digital Volume Correlation of in-situ loading using neutron tomography.* J Mech Behav Biomed Mater, 2017. **75**: p. 271-278.
168. Grandfield, K., et al., *Visualizing biointerfaces in three dimensions: electron tomography of the bone-hydroxyapatite interface.* J R Soc Interface, 2010. **7**(51): p. 1497-501.
169. Grandfield, K., S. Gustafsson, and A. Palmquist, *Where bone meets implant: the characterization of nano-osseointegration.* Nanoscale, 2013. **5**(10): p. 4302-8.
170. Sroka-Bartnicka, A., et al., *The biocompatibility of carbon hydroxyapatite/beta-glucan composite for bone tissue engineering studied with Raman and FTIR spectroscopic imaging.* Anal Bioanal Chem, 2015. **407**(25): p. 7775-85.
171. Gourion-Arsiquaud, S., et al., *Studying variations in bone composition at nano-scale resolution: a preliminary report.* Calcif Tissue Int, 2014. **95**(5): p. 413-8.
172. Mandair, G.S. and M.D. Morris, *Contributions of Raman spectroscopy to the understanding of bone strength.* Bonekey Rep, 2015. **4**: p. 620.
173. Raghavan, M., et al., *Age-specific profiles of tissue-level composition and mechanical properties in murine cortical bone.* Bone, 2012. **50**(4): p. 942-53.
174. Shah, F.A., et al., *3D printed Ti6Al4V implant surface promotes bone maturation and retains a higher density of less aged osteocytes at the bone-implant interface.* Acta Biomater, 2016. **30**: p. 357-367.
175. Krishna, B.V., S. Bose, and A. Bandyopadhyay, *Low stiffness porous Ti structures for load-bearing implants.* Acta Biomater, 2007. **3**(6): p. 997-1006.
176. Korabi, R., K. Shemtov-Yona, and D. Rittel, *On stress/strain shielding and the material stiffness paradigm for dental implants.* Clin Implant Dent Relat Res, 2017. **19**(5): p. 935-943.
177. Korabi, R., et al., *The Failure Envelope Concept Applied To The Bone-Dental Implant System.* Sci Rep, 2017. **7**(1): p. 2051.

178. Craven, T.G., et al., *The effects of implant stiffness on the bypassed bone mineral density and facet fusion stiffness of the canine spine.* Spine (Phila Pa 1976), 1994. **19**(15): p. 1664-73.
179. Simon, U., et al., *Influence of the stiffness of bone defect implants on the mechanical conditions at the interface--a finite element analysis with contact.* J Biomech, 2003. **36**(8): p. 1079-86.
180. Stoppie, N., et al., *The influence of Young's modulus of loaded implants on bone remodeling: an experimental and numerical study in the goat knee.* J Biomed Mater Res A, 2009. **90**(3): p. 792-803.
181. Gottlow, J., et al., *Evaluation of a new titanium-zirconium dental implant: a biomechanical and histological comparative study in the mini pig.* Clin Implant Dent Relat Res, 2012. **14**(4): p. 538-45.
182. Arabnejad, S., et al., *Fully porous 3D printed titanium femoral stem to reduce stress-shielding following total hip arthroplasty.* J Orthop Res, 2017. **35**(8): p. 1774-1783.
183. Lin, D.J., et al., *Bone formation at the surface of low modulus Ti-7.5Mo implants in rabbit femur.* Biomaterials, 2007. **28**(16): p. 2582-9.
184. Sumitomo, N., et al., *Experiment study on fracture fixation with low rigidity titanium alloy: plate fixation of tibia fracture model in rabbit.* J Mater Sci Mater Med, 2008. **19**(4): p. 1581-6.
185. Shi, L., et al., *The improved biological performance of a novel low elastic modulus implant.* PLoS One, 2013. **8**(2): p. e55015.
186. Kasemo, B. and J. Gold, *Implant surfaces and interface processes.* Adv Dent Res, 1999. **13**: p. 8-20.
187. Le Guehennec, L., et al., *Surface treatments of titanium dental implants for rapid osseointegration.* Dent Mater, 2007. **23**(7): p. 844-54.
188. Wennerberg, A. and T. Albrektsson, *On implant surfaces: a review of current knowledge and opinions.* Int J Oral Maxillofac Implants, 2010. **25**(1): p. 63-74.
189. Wennerberg, A. and T. Albrektsson, *Suggested guidelines for the topographic evaluation of implant surfaces.* Int J Oral Maxillofacial implants, 2000. **15**(3): p. 331-344.